AEROSPACE REPORT NO.
ATR-74(7416)-1

NASA CR-132452

Passive Suppression of Pogo on the Space Shuttle

Prepared by

M. H. Lock
and
S. Rubin
Vehicle Engineering Division

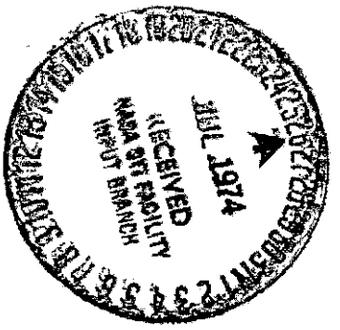

29 April 1974

Prepared for

LANGLEY RESEARCH CENTER
NATIONAL AERONAUTICS AND SPACE ADMINISTRATION
Langley Station, Hampton, Virginia

Contract No. NAS1-12215

Engineering Science Operations
THE AEROSPACE CORPORATION

(NASA-CR-132452) PASSIVE SUPPRESSION OF POGO ON THE SPACE SHUTTLE (Aerospace Corp., El Segundo, Calif.) 81 p HC $4.00 CSCL 22B

N74-29282

Unclas G3/31 43760

Aerospace Report No.
ATR-74(7416)-1

NASA CR-132452

PASSIVE SUPPRESSION OF POGO ON THE SPACE SHUTTLE

Prepared by

M. H. Lock
and
S. Rubin
Vehicle Engineering Division

29 April 1974

Engineering Science Operations
THE AEROSPACE CORPORATION
El Segundo, California

Prepared for

LANGLEY RESEARCH CENTER
NATIONAL AERONAUTICS AND SPACE ADMINISTRATION
Langley Station, Hampton, Virginia

Contract No. NAS1-12215

PASSIVE SUPPRESSION OF POGO ON THE SPACE SHUTTLE

Approved

S. Rubin, Senior Staff Engineer
Vehicle Integrity Subdivision
Vehicle Engineering Division

Passive Suppression of Pogo on the Space Shuttle

by

M. H. Lock and S. Rubin
The Aerospace Corporation

ABSTRACT

This study provides a qualitative assessment of (1) the tendency for pogo instability of the Shuttle vehicle in the absence of suppression devices and (2) the effectiveness of two passive suppressors (the compliant accumulator and the resistive accumulator) in counteracting any tendency toward instability. In addition, the relative effectiveness of three suppressor locations [the low pressure pump (LWOP) inlet and discharge and the high pressure pump (HPOP) inlet] is also evaluated.

The primary conclusion of the study is that effective pogo suppression, with passive devices, can be accomplished at the HPOP inlet location but not at the LPOP locations. Other conclusions are drawn regarding the relative effectiveness of the two accumulator types and with respect to tentative accumulator design requirements. Finally, a number of recommendations are made regarding future studies.

CONTENTS

SUMMARY 1

INTRODUCTION 2

NOMENCLATURE 4

1. DESIGN CRITERIA FOR RESISTIVE ACCUMULATOR 7
   1.1 Accumulator Model. 7
   1.2 Approximate Stability Analysis 8
   1.3 Design Criteria 10

2. ANALYTICAL MODEL FOR STABILITY ANALYSIS 13
   2.1 Shuttle Propulsion System/Structural Model 13
   2.2 Computational Procedure 13
   2.3 Numerical Values of System Parameters 15
      2.3.1 Propulsion-System Parameters 15
      2.3.2 Structural-Mode Data 16

3. SYSTEM STABILITY ANALYSIS 19
   3.1 Basic System 21
      3.1.1 Propulsion-System Modes 21
      3.1.2 Selection of Cases 23
      3.1.3 Stability Results 26
         3.1.3.1 Orbiter End-Burn 26
         3.1.3.2 Liftoff 26
         3.1.3.3 After SRB Separation 40
   3.2 System with Compliant Accumulator 40
      3.2.1 Propulsion-System Modes 40
      3.2.2 Selection of Cases 40
      3.2.3 Stability Results 44
         3.2.3.1 Orbiter End-Burn 44
         3.2.3.2 Liftoff 48
         3.2.3.3 After SRB Separation 48
   3.3 System with Resistive Accumulator 54
      3.3.1 Propulsion-System Modes 54
      3.3.2 Selection of Cases 54

CONTENTS (Continued)

3.3.3 Stability Results 57
3.3.3.1 Orbiter End-Burn 57
3.3.3.2 Liftoff 62
3.3.3.3 After SRB Separation 62

4. SUMMARY AND CONCLUSIONS 63

5. FUTURE STUDIES 65

APPENDICES:

A. SYSTEM EQUATIONS 66

B. SHUTTLE LOX SYSTEM PARAMETERS 72

REFERENCES 74

FIGURES

1.	Model for accumulator design criteria analysis	9
2.	Resistive accumulator design parameters	12
3.	Lox system elements of system stability model	14
4.	Variation of pump inlet cavitation compliance	17
5.	Variation of pump gain	18
6.	Variation of structural gain	20
7.	Lox system frequencies and damping ratios: orbiter end-burn	22
8.	Lox system modes: orbiter end-burn	24
9.	Stability results for basic system: orbiter end-burn	27
10.	Unstable mode of basic system: orbiter end-burn	33
11.	Stability results for basic system: liftoff	34
12.	Unstable mode of basic system: liftoff	41
13.	Stability results for basic system: after SRB separation	42
14.	Stability results with compliant accumulator: orbiter end-burn	45
15.	Variation of stability with compliant accumulator volume for HPOP inlet location: orbiter end-burn	47
16.	Fundamental mode stability with compliant accumulator: liftoff	49
17.	Variation of stability with compliant accumulator volume for HPOP inlet location: liftoff	50
18.	Stability results with compliant accumulator: liftoff	51
19.	Fundamental mode stability with compliant accumulator: after SRB separation	53
20.	Variation of stability with compliant accumulator volume for HPOP inlet location: after SRB separation	55
21.	Stability results with compliant accumulator: after SRB separation	56
22.	Stability results with resistive accumulator: orbiter end-burn	58

PASSIVE SUPPRESSION OF POGO ON THE SPACE SHUTTLE

by M. H. Lock and S. Rubin
The Aerospace Corporation

SUMMARY

This study provides a qualitative assessment of (1) the tendency for pogo instability of the Shuttle vehicle in the absence of suppression devices and (2) the effectiveness of two passive suppressors (the compliant accumulator and the resistive accumulator) in counteracting any tendency toward instability. In addition, the relative effectiveness of three suppressor locations [the low pressure pump (LPOP) inlet and discharge and the high pressure pump (HPOP) inlet] is also evaluated.

The assessments are made upon the basis of stability analyses undertaken with an idealized model of the Space Shuttle. Although an idealization, this model contained description of the higher organ-pipe modes of the feedline, an interpump mode of the oxidizer system, and the coupled longitudinal and lateral motions of the vehicle structure. The model is especially rigorous with regard to the feedline modes in that a continuous representation is employed. In addition, the generalized force contributions due to fluid resistance, fluid-momentum effects, turns in the fluid flow, and tank outflow effects are considered as well as the engine thrust contributions.

The results of the stability analyses revealed instabilities of the basic system (i.e., no suppressors) that involved the interpump mode as well as the feedline-type modes of the propulsion system. Both instabilities were found to be eliminated by the use of either compliant or resistive accumulators at the HPOP inlet. The use of these accumulators at either the LPOP inlet or discharge was found to aggravate the instability that involved the interpump mode. Accumulators at the LPOP inlet were found to eliminate the instabilities that involved the feedline-type modes of the propulsion system.

The primary conclusion of the study is that effective pogo suppression, with passive devices, can be accomplished at the HPOP inlet location but not at the LPOP locations. Other conclusions are drawn regarding the relative effectiveness of the two accumulator types and with respect to tentative accumulator design requirements. Finally, a number of recommendations are made regarding future studies.

INTRODUCTION

The suppression of pogo instability on the Space Shuttle is complicated by the nature of the vehicle structure and liquid propulsion system. In the case of the structure, the multibody configuration introduces significant coupling between the lateral and longitudinal motions of the vehicle. Since all such motions can couple with the propellant flows, the analysis of the pogo phenomenon on the Space Shuttle will require an accurate description of both lateral and longitudinal motions. In the case of the propulsion system, the length of the oxidizer feedline results in a number of higher organ-pipe hydraulic modes in the frequency range where strong structural/propulsion system interaction could occur, thereby raising the possibility of pogo instability over a broad range of modes and frequencies. In addition, the engine itself can introduce a propulsion-system mode that is primarily internal to the engine and which results from the presence of two pumps with a significant length of intermediate ducting. An unpublished study by S. Rubin has suggested that such an "interpump" mode of the oxidizer system can lead to instability. This latter circumstance raises a question about the location of a pogo suppression device since it is possible that a suppressor located at the inlet of the engine would not be effective in suppressing an instability that involves an interpump mode. Conversely, a suppressor located internal to the engine may not be effective in suppressing an instability that involves a feedline mode.

The goal of the present study is to provide judgments on the issues raised by the complexities of the Space Shuttle system. These judgments are developed from an analysis of the system which, although simplified, does contain an account of the lateral and longitudinal motions of the structure, the higher oxidizer feedline organ-pipe modes, and an interpump mode. Specifically, the study is directed at (1) an examination of the tendency for pogo instability of the Shuttle vehicle in the absence of suppression devices, (2) an evaluation of two passive accumulator types,* compliant and resistive, and (3) an evaluation of three accumulator locations.

The compliant accumulator (no inertance or resistance) is a simplification of the type of device commonly used on past vehicles. These devices were, in general, intended to be purely compliant but, in fact, possessed some small inherent inertance and resistance. The resistive accumulator (substantial resistance, along with inertance and compliance) was introduced quite recently on the Delta Stage I vehicle to help correct a problem that had arisen due to significant spatial separation between the accumulator and the engine inlet (ref. 1). This separation introduced a second hydraulic mode of the feed-system that led to instability.

The consequences of the Delta Stage I instability were ameliorated with the introduction of significant resistance by means of the accumulator.

---

*A companion study (NAS3-17758) is being undertaken on the use of active suppressors.

Although the device had been introduced for a problem that resulted from accumulator/pump separation, the character of the device indicated that it could provide system damping over a wide frequency range irrespective of accumulator/pump separation. This feature of the resistive accumulator made it appear an attractive candidate for use on the Space Shuttle and led to its selection for examination in the present study. For simplicity, the present study only treated the case of zero accumulator/pump separation. The examination of the consequences of finite separation (applicable for both resistive and compliant devices) is considered more appropriate for later more refined studies.

With respect to the evaluation of accumulator location, it was decided to perform stability analyses with both accumulator types at the following three locations:

1. Low-pressure pump inlet
2. Low-pressure pump discharge
3. High-pressure pump inlet

The results obtained for these cases were also compared against the corresponding results for the basic system (i.e., the vehicle without suppressors). The analyses were undertaken for the oxidizer system alone since unpublished preliminary studies by the Rockwell International Space Division have indicated that this portion of the propulsion system is most likely to be critical from the standpoint of pogo instability.

The subsequent sections of the report describe the development of design criteria for the resistive accumulator, the formulation of the analytical model for the stability analyses, and the stability analyses of the basic system and the system with incorporation of the compliant and resistive devices. The results are summarized, conclusions are drawn, and recommendations made for future studies.

The authors would like to acknowledge the work of Raymond E. Orth and Heather Bagwell in the programming of the system stability equations and the propulsion system equations, respectively.

NOMENCLATURE

Units: M (mass), F (force), L (length), T (time)

a	acoustic velocity $[LT^{-1}]$
A	area $[L^2]$
A_T	effective area of thrust chamber $[L^2]$
B	see eq. (1.3)
C	compliance, $[F^{-1}L^5]$
C_f	thrust coefficient, [–]
D	see eq. (1.3)
$\bar{f}$	mean mass flow of propellant, $[MT^{-1}]$
g	standard acceleration of gravity, $[LT^{-2}]$
G_e	structural gain for engine motion, $\phi^2(e)/M$, $[M^{-1}]$
h_t	height of propellant in tank, [L]
h_s	height of tank-to-engine feedline, [L]
i	imaginary unit, $\sqrt{-1}$
ℓ	line length, [L]
L	inertance, $[FL^{-5}T^2$ or $ML^{-4}]$
$m+1$	pump dynamic gain, [–]
M	mass, [M]
M_n	generalized mass of nth structural mode, [M]
$\mathscr{P}_n$	modal tank-bottom pressure per unit acceleration of generalized coordinate, $[FL^{-3}T^2]$
P	oscillatory pressure, $[FL^{-2}]$
q_n	generalized displacement of nth structural mode
Q	volumetric flow, $[L^3T^{-1}]$

R	resistance, $[FL^{-5}T]$
s	Laplace variable used to denote the complex frequency $\sigma + i\omega$, $[T^{-1}]$
t	time, $[T]$
T	thrust, $[F]$
x	structural displacement along longitudinal axis, $[L]$
z	structural displacement along lateral axis, $[L]$
$\bar{V}$	steady flow velocity of propellant $[LT^{-1}]$
Y	flow admittance, $[F^{-1}L^{5}T^{-1}]$
Z	flow impedance, $[FL^{-5}T]$
α_{ij}	coefficients in feedline transmission function; see Appendix A [–]
ζ	ratio of critical damping for structural mode, [–]
ζ_a	ratio of critical damping for accumulator [–]
ζ_N	structural damping required for neutral system stability, [–]
θ	complex propagation angle
ρ	propellant mass density, $[ML^{-3}]$
τ	travel time in a hydraulic line, $\sqrt{LC}$ or ℓ/a, $[T]$
ϕ_n	modal displacement, [–]
ω	angular frequency, $[T^{-1}]$
ω_a	natural frequency of the accumulator $[T^{-1}]$
ω_n	natural frequency of structural mode, $[T^{-1}]$
Ω	frequency ratio; see eq. (1.5) [–]

Subscripts

a	accumulator
b	bubble
c	chamber

d	discharge
e	engine
ip	interpump
ℓ	lower limit
n	nth structural-system mode
p	pump
R	real part; relative
t	tank
u	upper limit

1. DESIGN CRITERIA FOR RESISTIVE ACCUMULATOR

The objective of the use of the resistive accumulator is to produce a significant level of hydraulic damping over a specified frequency range. This section of the report provides a measure of the required level of damping and develops accumulator design criteria for achieving the desired characteristics.

1.1 Accumulator Model

The accumulator is assumed to be a linear device characterized by an inertance, L_a, a compliance, C_a, and a resistance, R_a. Assuming time-dependent perturbations of the form e^{st}, where s is the Laplace variable, the equations governing the accumulator can be written

$$s\, L_a Q_a + R_a Q_a = P_a - P \tag{1a}$$

$$Q_a = - s\, C_a P_a \tag{1b}$$

where Q_a is the volume flow out of the accumulator, P_a is the accumulator internal pressure, and P is the pressure at the entrance to the accumulator (see sketch).

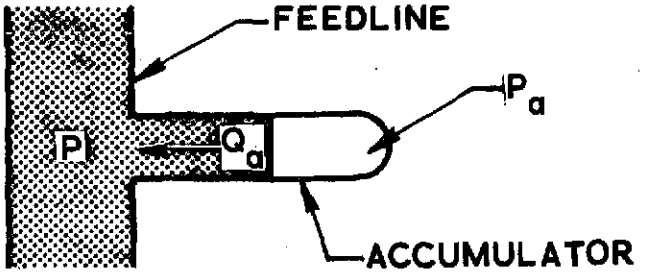

The flow admittance, Y_a, of the accumulator can be written

$$Y_a = - \frac{Q_a}{P} = \frac{s}{L_a} \left\{ s^2 + 2\, \zeta_a \omega_a\, s + \omega_a^2 \right\}^{-1} \tag{2}$$

where the accumulator natural frequency, ω_a, and damping ratio, ζ_a, are defined by

$$\omega_a^2 = \frac{1}{L_a C_a}\,; \quad \zeta_a = \frac{R_a C_a \omega_a}{2}$$

1.2 Approximate Stability Analysis

The basis for the design criteria for the resistive accumulator was developed from an approximate stability analysis of the single-pump system shown in figure 1. The analysis was undertaken under the assumption that the structural system responds in a single mode. Employing the approximate method of reference 2, the structural damping required for neutral stability, ζ_N, is found to be given by

$$\zeta_N \approx \frac{(m+1)BG_e}{\left\{R_e \text{ Real } Y_a + (m+1)\right\}} \frac{(1-D)}{2\omega_n} \tag{3}$$

where

$$B = A_l A_T R_c \left(1 + \frac{h_t}{h_s} \frac{\phi_t}{\phi_e}\right)$$

$$D = \frac{A_l R_e}{(m+1)A_T R_c} \frac{\phi_e}{\phi_t}$$

and where

A_l	=	cross-sectional area of feedline
h_s	=	length of feedline
h_t	=	height of fluid in tank
R_e	=	engine resistance
R_c	=	thrust-chamber resistance
A_T	=	effective area of thrust chamber (i.e., area x thrust coefficient)
$(m+1)$	=	gain of pump
ϕ_e	=	modal displacement of engine
ϕ_t	=	modal displacement of center of gravity of propellant in tank
ω_n	=	frequency of the structural mode involved

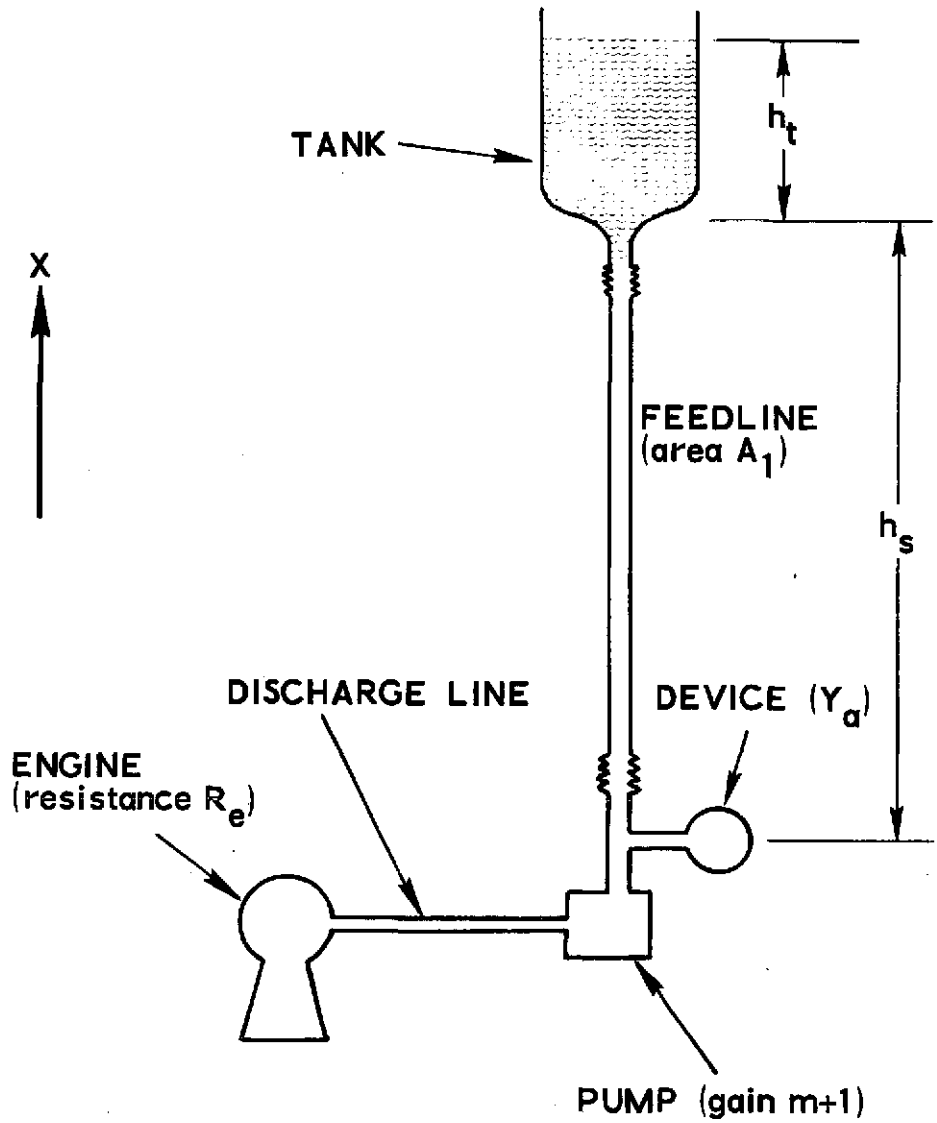

Figure 1. Model for accumulator design criteria analysis

The structural gain, G_e, for longitudinal motion of the engine is defined by

$$G_e = \frac{\phi_e^2}{M}$$

where M is the generalized mass of the structural mode.

1.3 Design Criteria

The form of equation (3) indicates that the structural damping required for neutral stability will decrease with increase of the real part of the accumulator admittance. The equation also indicates that the magnitude of this term should be such that

$$\text{Real } Y_a >> (m+1)/R_e \tag{4}$$

for the resistive accumulator to be effective. Therefore, the design goal for the accumulator is to maintain the inequality [eq. (4)] over the frequency range of interest.

For the case of harmonic oscillations at the frequency, ω, the real part of the admittance, Y_a, can be written

$$\text{Real } Y_a = \frac{2\zeta_a}{\omega_a L_a} \left\{ \left(\frac{1}{\Omega} - \Omega \right)^2 + (2\zeta_a)^2 \right\}^{-1} \tag{5}$$

where the frequency ratio $\Omega = \omega/\omega_a$. The derivative of Real Y_a with respect to Ω is

$$\frac{d}{d\Omega} \text{Real } Y_a = \frac{4\zeta_a (1-\Omega^4)}{\omega_a L_a \Omega^3 \left| (1/\Omega - \Omega)^2 + (2\zeta_a^2) \right|^2} \tag{6}$$

The results [eqs. (5) and (6)] indicate that Real Y_a increases monotonically to a maximum at Ω equal to unity and then decreases monotonically as Ω increases above unity. The maintainance of Real Y_a above some selected value, say α, over the frequency range, $\omega_\ell \leq \omega \leq \omega_u$, is assured if

$$\text{Real } Y_a(\omega_\ell) \geq \alpha \tag{7a}$$

$$\text{Real } Y_a(\omega_u) \geq \alpha \tag{7b}$$

The conditions [eq. (7)] then lead to the following requirements on the accumulator parameters

$$\omega_\ell C_a \sqrt{R_a \alpha (1 - R_a \alpha)} \geq \alpha \left| 1 - \omega_\ell^2 L_a C_a \right| \tag{8a}$$

$$\omega_u C_a \sqrt{R_a \alpha (1 - R_a \alpha)} \geq \alpha \left| 1 - \omega_u^2 L_a C_a \right| \tag{8b}$$

The requirements [eq. (8)] constitute the design criteria for the resistive accumulator. For a specified design goal these inequalities define a region of the accumulator parameters within which the design goal is satisfied. The application of the criteria is illustrated below for the design goal that was used subsequently in the study. This goal was

$$\text{Real } Y_a \geq 0.06 \text{ m}^5/\text{MN s } (1 \text{ in.}^2/\text{sec}) \text{ for } 2 \leq f \leq 30 \text{ Hz}^* \tag{9}$$

The allowable ranges of the accumulator parameters are most readily obtained by specifying the accumulator compliance, C_a, and then using equations (8a) and (8b) to define an allowable region of inertance, L_a, and resistance, R_a. A representative range of the accumulator compliance was taken to be from 0.006 m^5/MN (0.1 $in.^2$) to 0.12 m^5/MN (2.0 $in.^2$). This range was determined by enveloping compliance values that were estimated for a representative 0.057 m^3 (2 ft^3) volume accumulator using propulsion system pressure data supplied by Rockwell. The resulting regions of allowable values of inertance and resistance are shown in figure 2 together with a smaller region that was calculated for the condition Real $Y_a \geq 0.3$ m^5/MN s (5 $in.^2$/sec), also for $2 \leq f \leq 30$ Hz. From the figure, it is seen that the zones are relatively insensitive to the value of the accumulator compliance (at least for the range that was considered) but are quite sensitive to the selected level of the admittance. Insofar as an accumulator design is concerned, the selection of any combination of inertance and resistance values that are within the zone defined by curve A (fig. 2) will lead to satisfaction of the design goal [eq. (9)]. The particular combination that was selected for use in the stability analyses was

$$R_a = 1.7 \text{ MN s/m}^5 \ (0.1 \text{ sec/in.}^2)$$

$$L_a = 0.023 \text{ MN s}^2/\text{m}^5 \ (0.00133 \text{ sec}^2/\text{in.}^2)$$

These values were judged to be practically achievable on the basis of Delta Stage I vehicle experience (ref. 1). In addition to this particular design, a number of other resistive accumulator designs were briefly examined to determine the sensitivity of the stability results to the accumulator parameters.

*The admittance in SI units is based upon volume flow divided by pressure; in English units, weight flow is employed. This flow difference also applies to the resistance and inertance units.

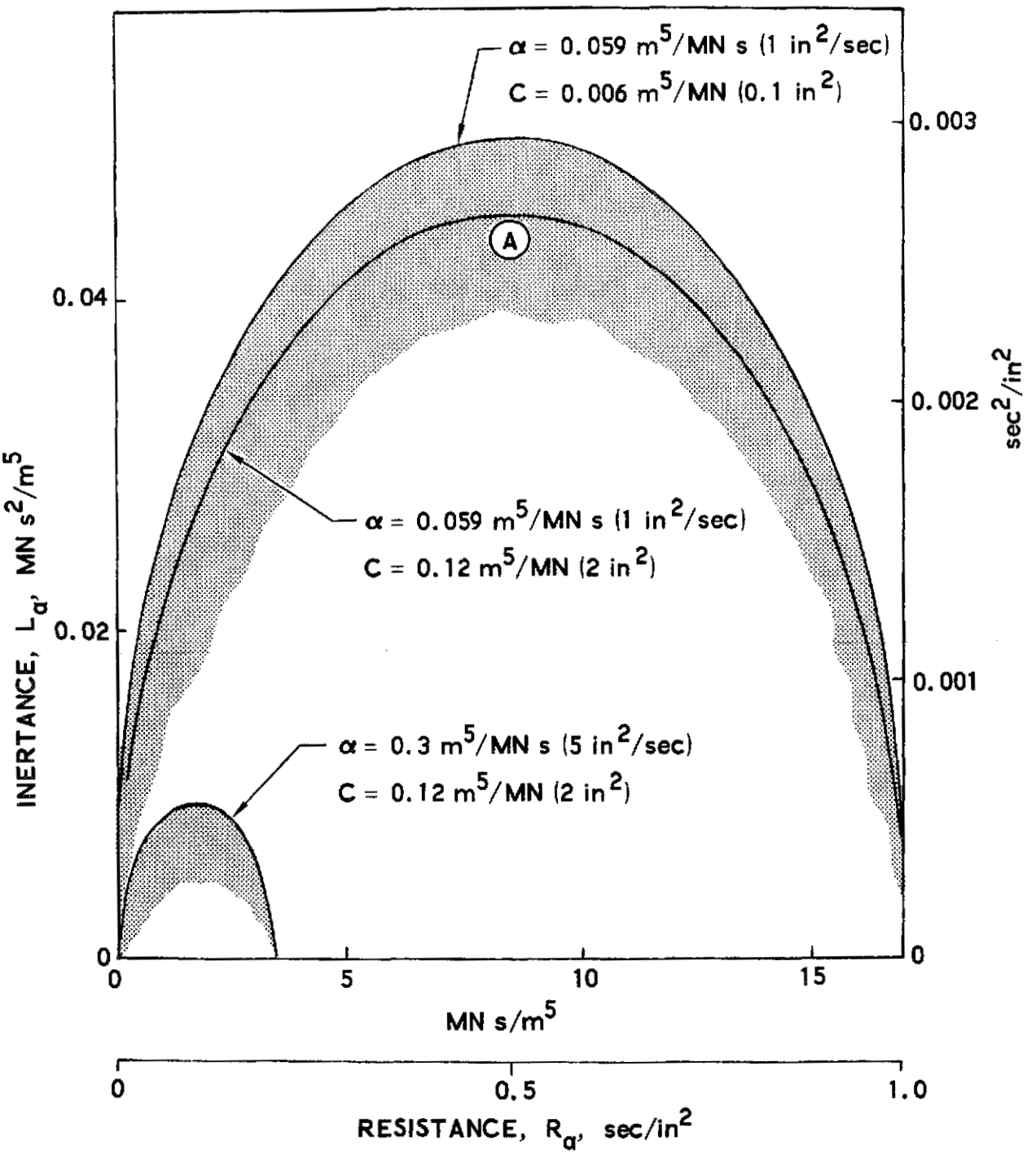

Figure 2. Resistive accumulator design parameters

2. ANALYTICAL MODEL FOR STABILITY ANALYSIS

2.1 Shuttle Propulsion System/Structural Model

For the purpose of the stability analysis, the most important features of the vehicle propulsion system were represented using a single equivalent engine. The elements employed are shown in figure 3 and consist of a lox tank, two feedline segments (one longitudinal and one lateral), a low-pressure pump (LPOP), an interpump line, a high-pressure pump (HPOP), a discharge line, an injector, and a combustion chamber. For the purposes of the present study, the motion of the Shuttle vehicle was represented by a single structural mode. This representation was considered adequate except for the exceptional case of proximate structural modes (i.e., modes with very close frequencies) with comparable gains. As a consequence of this representation, the structural modes selected for use in the stability analysis were examined one at a time.

The detailed equations that govern the motion of the system are provided in Appendix A of this report. In order that these equations provide a representative description of the higher organ-pipe modes of the feedline, the exact solutions for a continuous hydraulic representation (including resistance) were employed to develop feedline transmission functions. This results in the appearance of hyperbolic functions of complex argument in the system equations. Since the wave transit times associated with the interpump and discharge lines were relatively short compared to the structural response times of interest, the fluids in these latter lines were treated as incompressible. Generalized force contributions that result from fluid resistance as well as from the convective derivative ($v\partial v/\partial x$, where v is the velocity of the flow) that appears in the fluid momentum equation were also included in the system equations.

On the assumption that the structural modes are developed with closed-bottom tanks, tank outflow effects are included (ref. 3). All corner forces at turns in the flow and drag forces across resistive elements are also included.

2.2 Computational Procedure

For the purpose of the stability calculations the equations of motion were reduced to a 14^{th} order system with the form

$$\left\{[V(s)] + [E][F(s)]\right\} \hat{H} = 0 \qquad (10)$$

where the matrix $[V(s)]$ describes the basic coupled structure/propulsion system (i.e., the system in the absence of accumulators); the matrix $[E]$

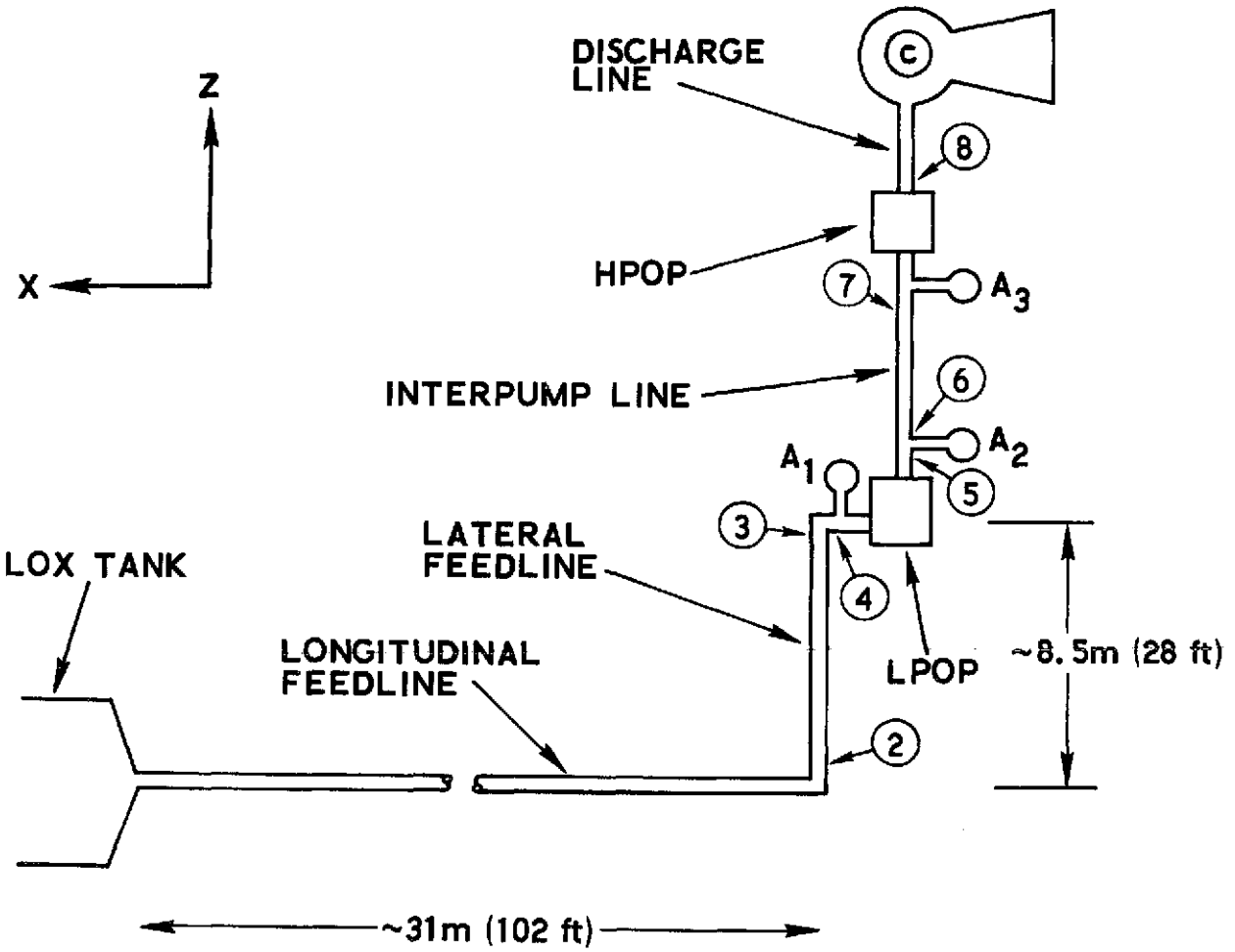

Figure 3. Lox system elements of system stability model

provides the specification of the accumulator location while the matrix $[F(s)]$ contains the description of the accumulator characteristics. The solution vector $\hat{H}$ comprises

$$\hat{H} = \left| P_2, P_4, P_5, P_7, P_8, P_c, Q_t, Q_2, Q_3, Q_4, Q_5, Q_7, Q_8, q_n \right| \tag{11}$$

where P_j and Q_j denote the pressures and flows at various points within the oxidizer system (fig. 3). The q_n term is the generalized coordinate associated with the n^{th} structural mode; the motion $\vec{x}$ of the vehicle at some point $\vec{r}$ is related to q_n by the following:

$$\vec{x} = q_n e^{st} \phi_n(\vec{r})$$

where $\phi_n(\vec{r})$ is the structural mode shape and s is the Laplace variable.

The matrix equations are completely defined when the propulsion-system parameters and structural-mode data are specified. When this is done, the eigenvalues, s_i, and corresponding eigenvectors, $\hat{H}_i$, of the system can be obtained by satisfaction of the conditions

$$\det \left| [V(s_i)] + [E][F(s_i)] \right| = 0 \tag{12a}$$

$$\left| [V(s_i)] + [E][F(s_i)] \right| \hat{H}_i = 0 \tag{12b}$$

Because of the use of the exact feedline solutions the determinantal equation is a transcendental equation in the Laplace variable. The eigenvalues of the equation were obtained with the use of an iterative root-finding subroutine (ref. 4) that used the input structural frequency, ω_n, and previously calculated propulsion-system eigenvalues as initial guesses.

2.3 Numerical Values of System Parameters

2.3.1 Propulsion-System Parameters

The cross-sectional areas and lengths of the various lines were based upon available Space Shuttle design data. The resistance and inertance of the lines, pumps, engine, and thrust chamber were developed from the basic data given in the SSME Engine Dynamic Model (ref. 5) and from information in a previous pogo study (ref. 3). The estimated values of these parameters are provided in Appendix B. The variation, with time of flight, of the cavitation bubble compliance at the pump inlets and of the pump gains were estimated from available operating data; the compliance estimates were made using the results presented in reference 3 (obtained from the "stay-time" method of ref. 6) and the pump gain from unpublished Titan and Delta

vehicle studies. The resulting time variations are shown in figures 4 and 5. The compliance and gain values employed in the stability analyses at specific flight times were taken from these figures.

2.3.2 Structural-Mode Data

The structural-mode data employed in the stability analyses were taken from a set of modal calculations undertaken by Rockwell. These calculations had been performed for the case of symmetric vibrations of the vehicle (i.e., no yaw motion) and were based upon a vehicle configuration (designated M89B) that was current in early 1973. The data were considered to be the best that were available for the present study. It may be noted in passing, that the Space Shuttle vehicle has subsequently been reduced in size and weight; however, modal data for the new configuration were not available for this study. The Rockwell data comprised the frequencies and mode shapes of the first hundred symmetric vibration modes at five specific flight conditions; in addition to the structural data, the lox tank-bottom displacements and pressures were also provided. The set of conditions treated by Rockwell is given in the table below together with the associated times of flight and the corresponding maximum and minimum values of the calculated frequencies; the abbreviation SRB that appears in the table denotes the solid-rocket booster.

Condition	Flight Time (sec)	Frequency (Hz)	
		f_1	f_{100}
Liftoff	0	2.18	44.5
Max. Dynamic Pressure	54	2.24	48.9
Before SRB Separation	116^-	2.28	53.3
After SRB Separation	116^+	2.29	62.4
Orbiter End-Burn	480	2.81	103.8

Examination of the modal data from the standpoint of structural gain indicated that the higher gain levels were associated with modal frequencies above 20 Hz. Based upon this feature of the calculated results and the increasing uncertainty of the data for the higher modes, a frequency of 30 Hz was selected as a reasonable upper limit to the frequency range to be considered in the subsequent stability analyses. The data also indicated that the higher levels of the structural gain, in the frequency range of interest, tended to be relatively insensitive to time of flight. This feature is

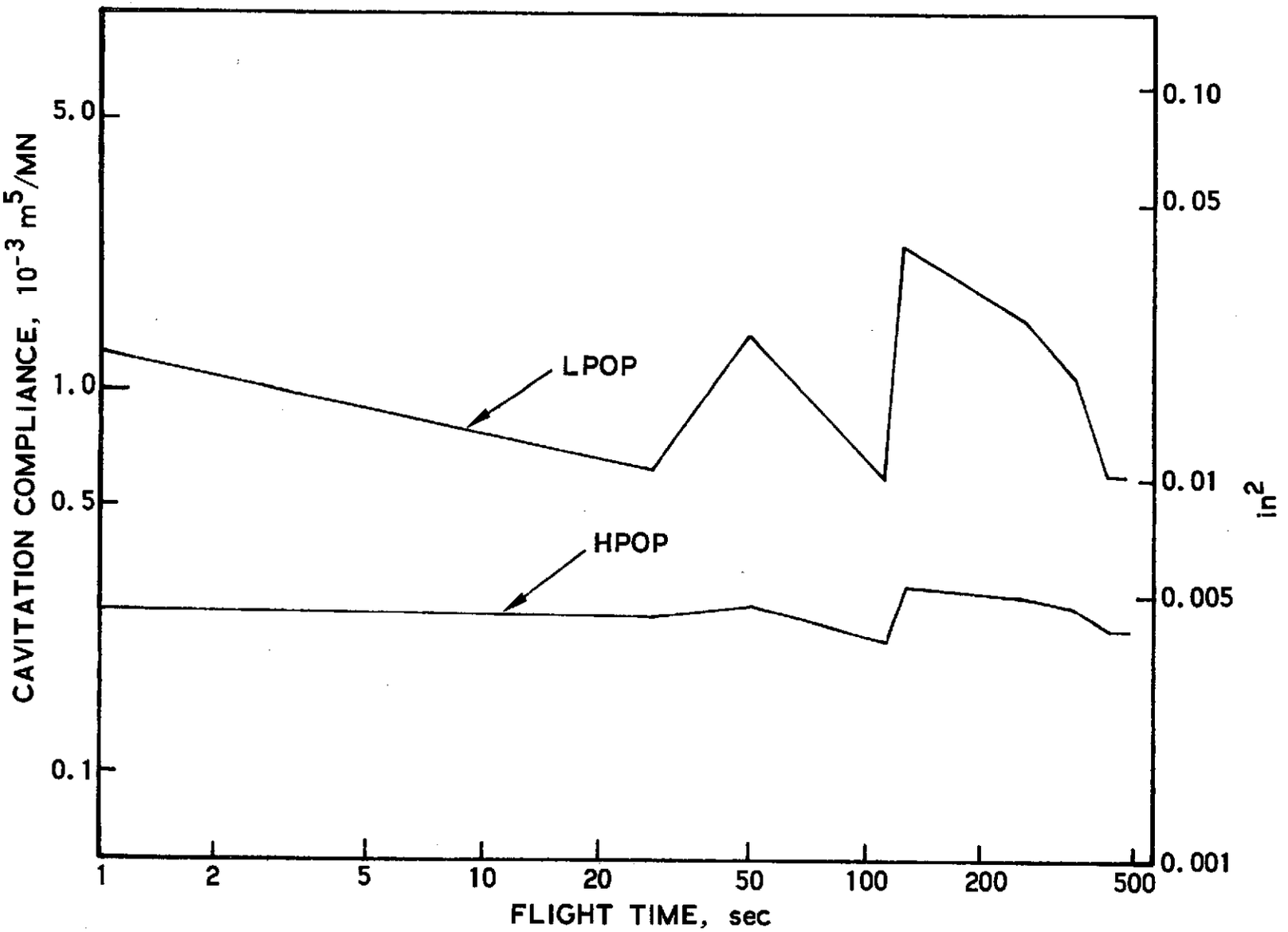

Figure 4. Variation of pump inlet cavitation compliance

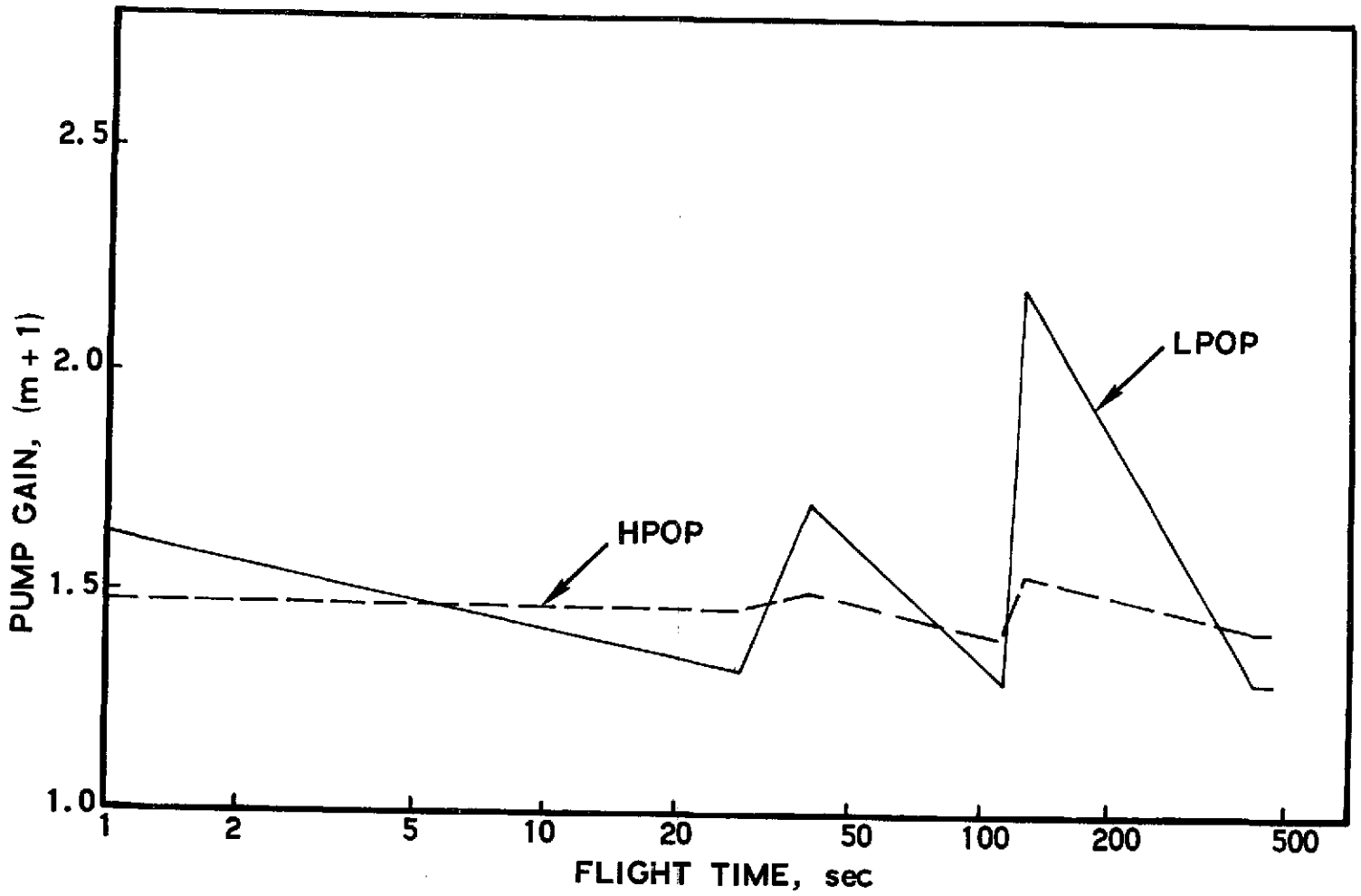

Figure 5. Variation of pump gain

illustrated in figure 6 where the variation with flight time of the two largest structural gains is presented; for comparison of relative magnitudes the gain in the fundamental mode is also shown. In the figure the higher gains have been identified by the approximate frequency of the structural mode. With the exception of one case, the gains are associated with a single mode. The exceptional case occurred at the orbiter end-burn condition where two proximate modes, one at 26.8 Hz and the other at 27.2 Hz both exhibited large structural gains of comparable magnitude.

For application in the stability analysis, the calculated structural-mode frequencies were allowed to vary through some ±15 percent. This variation was introduced to provide at least some account for changes in vehicle configuration and also uncertainties in the structure/propulsion-system modeling. The variation was expected to cover the worst case conditions in terms of the proximity of structural and propulsion resonances. To account for damping in the vehicle, a critical damping ratio of 0.01 was assigned to each structural mode.

Since the stability analysis is based upon a single equivalent system with three identical engines, the engine modal amplitude, ϕ_e, used in the stability calculations is related to the modal data by

$$\phi_e^2 = \frac{1}{3} \sum_{i=1}^{3} \phi_{ei}^2$$

where the ϕ_{ei} are the modal amplitudes of the individual engines. In a similar manner the tank-bottom pressure excitation $\mathscr{P}_n$ used in the analysis is related to the corresponding modal data $\mathscr{P}$ by

$$\mathscr{P}_n = \frac{\mathscr{P}}{3\phi_e} \sum_{i=1}^{3} \phi_{ei}$$

3. SYSTEM STABILITY ANALYSIS

To initiate the study, the following three suppressor configurations were analyzed:

1. Basic system (i.e., no pogo suppressor)
2. System with 0.057 m^3 (2 ft^3) volume compliant accumulator
3. System with 0.057 m^3 (2 ft^3) volume resistive accumulator designed to meet the requirements: Real $Y_a \geq 0.06$ $m^5/MN\ s$ (1 $in.^2/sec$) for $2 \leq f \leq 30$ Hz.

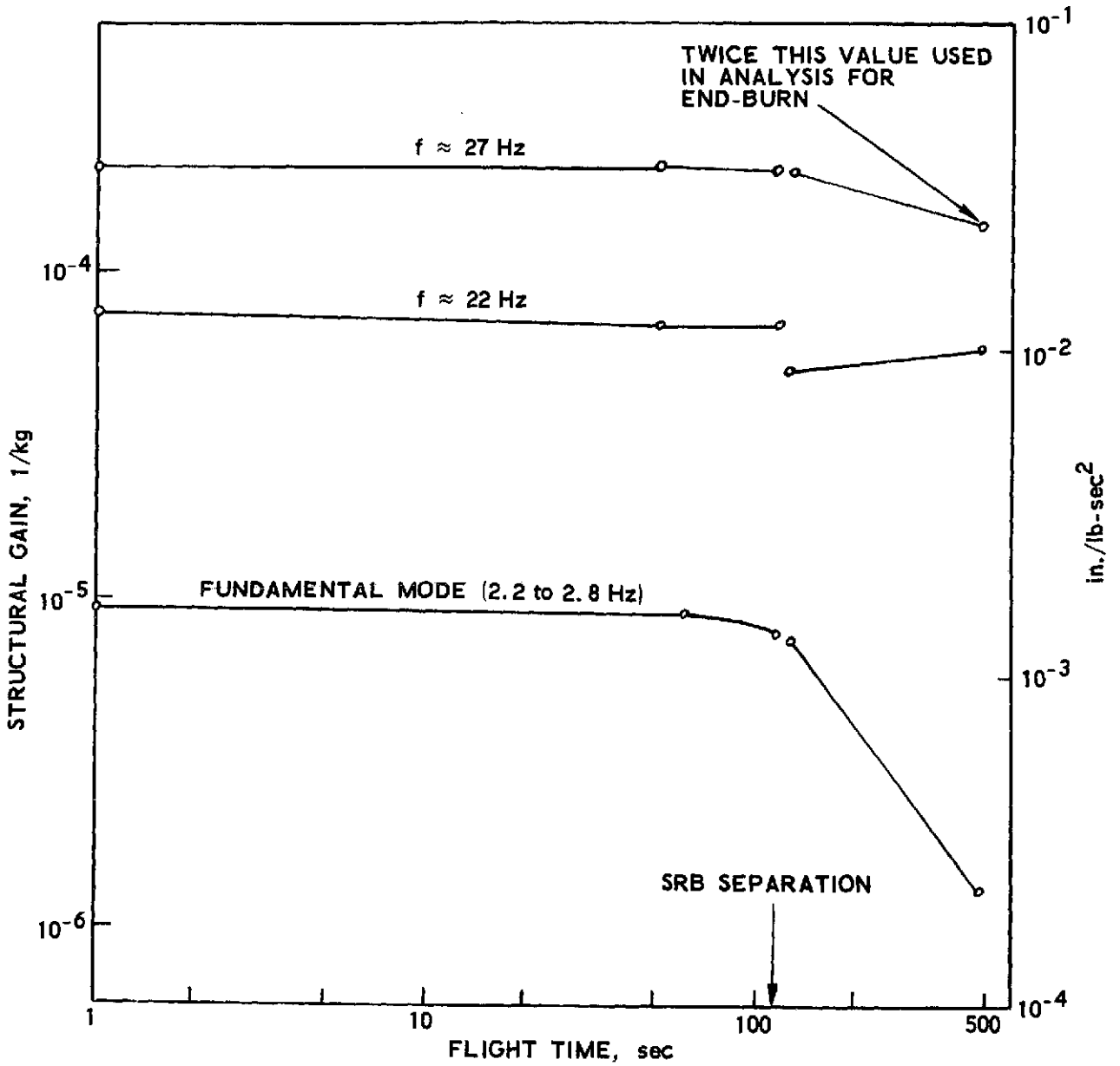

Figure 6. Variation of structural gain

The 0.057 m^3 (2 ft^3) volume used for both the resistive and compliant accumulators was chosen as a representative practical value. The condition on Real Y_a for the resistive accumulator was based upon an estimated magnitude of 0.008 m^5/MN s (0.14 $in.^2$/sec) for the comparable propulsion-system term $(m+1)/R_e$. Thus, the design ensures that Real $Y_a >> (m+1)/R_e$ over the frequency range of interest.

3.1 Basic System

3.1.1 Propulsion-System Modes

The eigenvalues and eigenvectors of the isolated propulsion system (i.e., stationary structure) were calculated both to provide initial guesses for the root-finding program used in the subsequent stability analysis and to identify the interpump mode of the propulsion system. The calculations were made using the numerical data given in Appendix B together with cavitation compliance and pump gain values taken from figures 4 and 5; the values of these latter items for the orbiter end-burn, liftoff and after SRB separation conditions are given in the following table.

Item \ Case	Liftoff	After SRB Separation	End-Burn
LPOP Gain (m_1+1)	1.625	2.2	1.306
HPOP Gain (m_2+1)	1.48	1.54	1.42
LPOP Inlet, C_{b1} $(10^{-3}m^5/MN)$	1.2	2.3	0.59
$(in.^2)$	(0.0204)	(0.039)	(0.01)
HPOP Inlet, C_{b2} $(10^{-3}m^5/MN)$	0.27	0.3	0.24
$(in.^2)$	(0.0045)	(0.0051)	(0.004)

The modal frequencies and the associated critical damping ratios calculated for the orbiter end-burn condition are presented graphically in figure 7. The results for the other flight conditions are similar. The interpump mode is noted in this figure. It is seen to be relatively highly damped with a frequency of 24.4 Hz (the frequency of this mode at the liftoff and after SRB separation conditions was 23.1 and 21.6 Hz, respectively). This resonance can be viewed simply as involving the interpump and LPOP fluids moving on

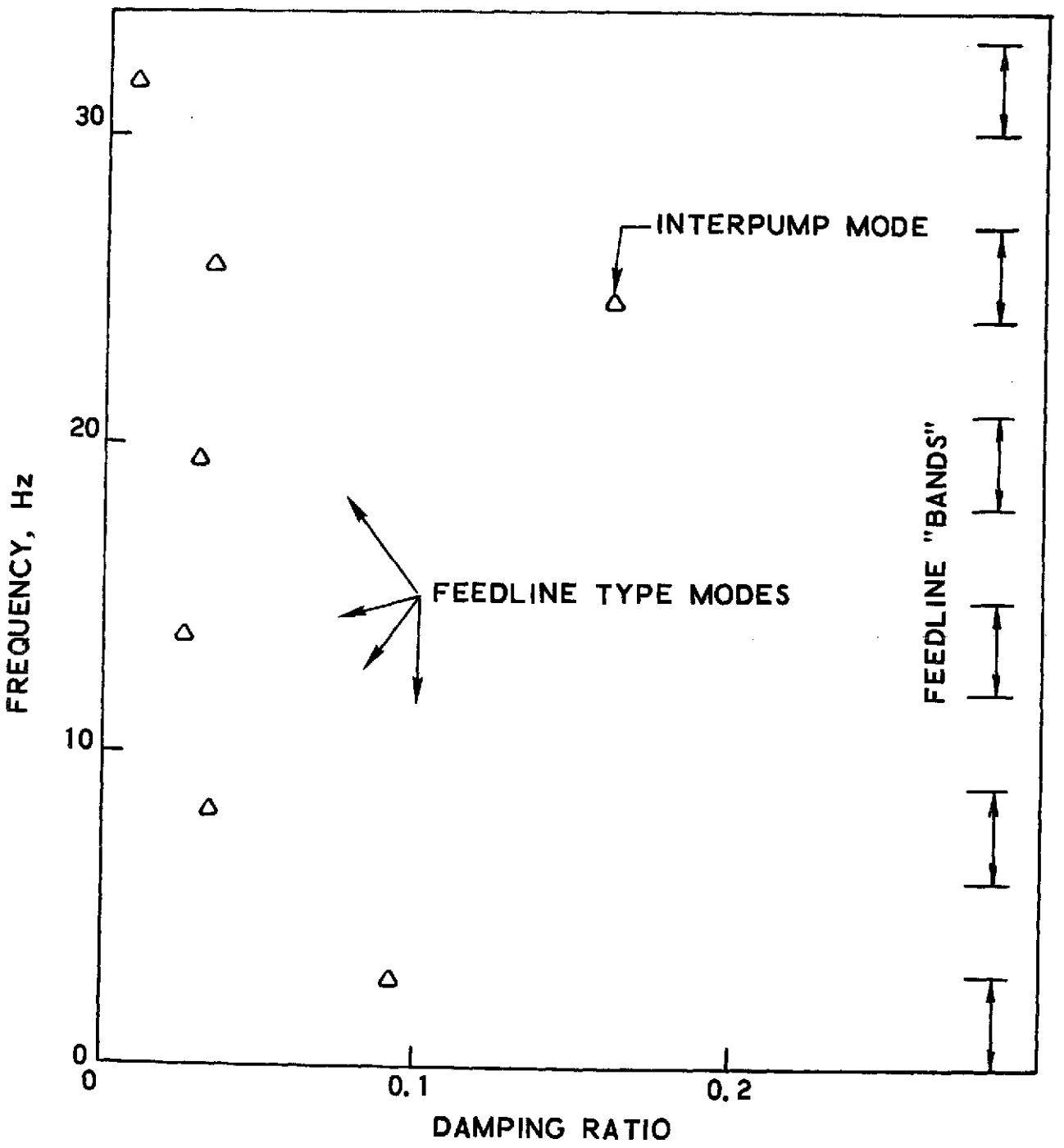

Figure 7. Lox system frequencies and damping ratios: orbiter end-burn

the LPOP inlet cavitation bubble compliance at the upstream end and the HPOP inlet cavitation bubble compliance at the downstream end (fig. 3). Consequently, the resonant frequency can be estimated with the formula

$$f_{ip}(\text{Hz}) \approx \frac{1}{2\pi}\left(\frac{1/C_{b1} + 1/C_{b2}}{L_i + L_{pi}}\right)^{1/2}$$

where L_i, L_{pi} denote the inertance of the interpump line and the LPOP, respectively; and where C_{b1}, C_{b2} denote the cavitation bubble compliance values at the inlet to the LPOP and HPOP, respectively. The above expression provides a means of gaging the sensitivity of this modal frequency to changes in the involved parameters. The remaining oxidizer system modes can be considered as "feedline-type" modes since their frequencies lie within the frequency bands defined by the open-open and open-closed modes of the feedline. The different character of the modes is illustrated in figure 8 where representative fluid pressure amplitude distributions are shown for the interpump mode and the first two feedline-type modes; the in or out phasing, shown crudely, approximates the actual phasing. The appearance of significant amplitudes only within the engine (i.e., beginning with the LPOP) for the interpump mode is clearly seen from the figure.

3.1.2 Selection of Cases

A particular stability case for the basic system comprised a specified flight condition and a specified structural mode. For a given case, the stability calculations were performed over the assumed ±15 percent variation in the structural mode frequency. Selection of the stability cases, particularly the selected structural modes, was largely governed by the character of the modal data; the modes with the higher structural gains being the candidates for the analysis. The end-burn condition was selected for initial analysis. The set of modes employed for analysis of end-burn stability are given in the table below, with the associated modal frequencies and the structural gains. In the table the nomenclature E denotes end-burn while the numbers give the order of the mode.

Item \ Mode	E1	E2	E7	E30	E34	E35
f_n(Hz)	2.8	4.7	8.5	22.5	26.8	27.2
$G_e(10^{-6}/\text{kg})$	1.25	1.14	6.3	57	177	274
(10^{-4} in./lb-sec^2)	(2.2)	(2.0)	(11)	(100)	(310)	(480)

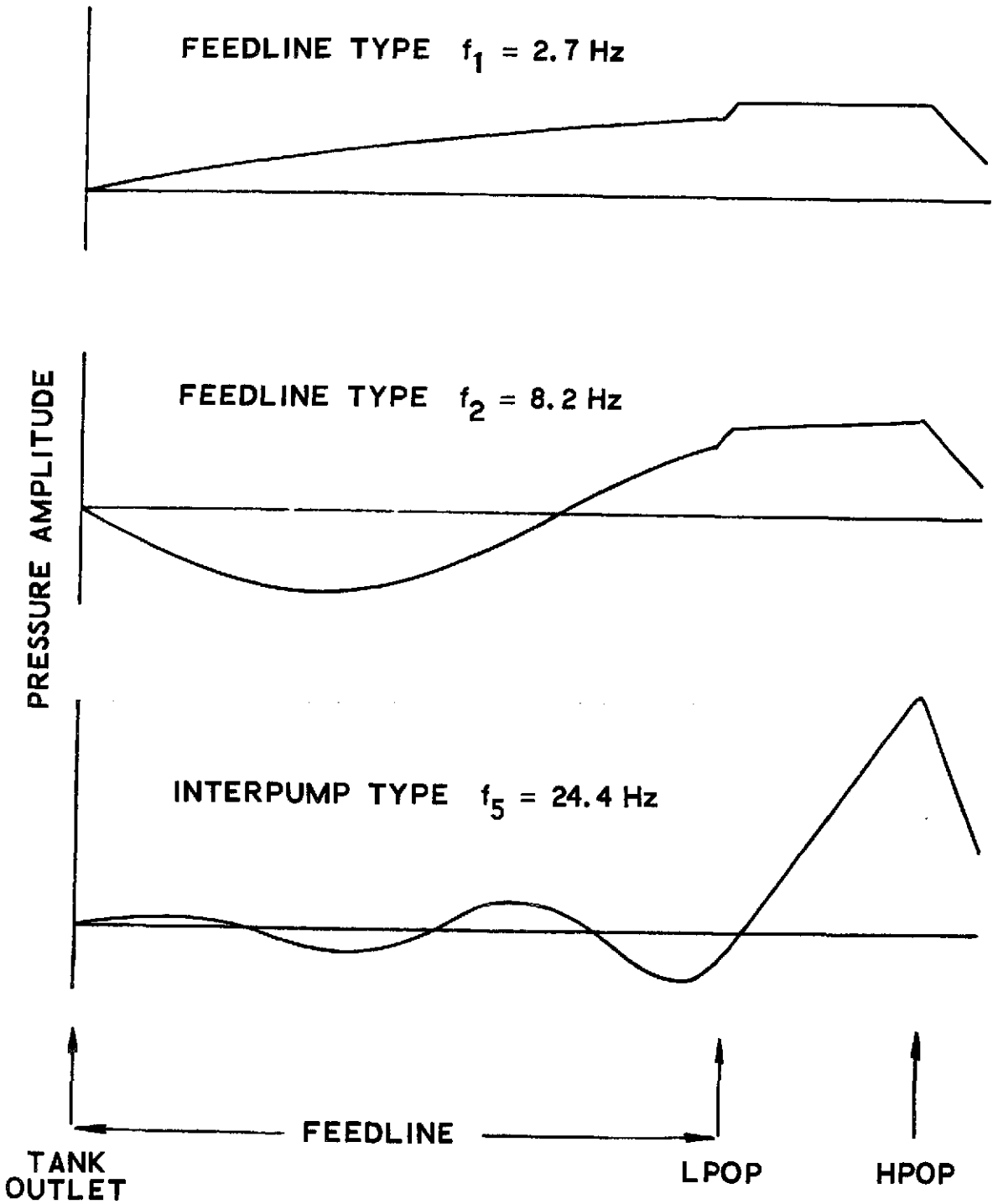

Figure 8. Lox system modes: orbiter end-burn

It should be noted that the structural gains assigned to the thirty-fourth and thirty-fifth modes are twice the values given by the modal data. This was done to account for the possibility of destabilizing coupling between the modes. Such coupling could not be described by the present analysis since it involved only a single structural mode. The use of a factor of two did not seem unreasonable since the two structural gains are of a comparable order of magnitude.

The tank-pressure excitation at the orbiter end-burn condition was assumed to be negligible. Since the absence of this excitation at end-burn could tend to de-emphasize the role of the feedline-type modes, it was clearly necessary to treat at least one earlier flight time where this excitation was present. The condition initially selected was liftoff where six structural modes were considered in the stability analyses. These modes with their associated frequencies and structural gains are given in the table below together with the corresponding values of the modal tank-bottom pressure per unit engine acceleration, $\mathscr{P}_n/\phi_e$.

Item \ Mode	L1	L18	L26	L49	L51	L62
f_n (Hz)	2.2	8.9	12.1	21.9	22.5	27.1
G_e (10^{-6}/kg)	9.1	4.6	11.4	74	8.6	206
(10^{-4} in./lb-sec^2)	(16)	(8)	(20)	(130)	(15)	(360)
$\mathscr{P}_n/\phi_e$ (Ns^2/m^3)	115	5.7	3.0	820	7640	-1.0
(10^{-5} lb-sec^2/in.^{3})	(42)	(2.1)	(1.1)	(300)	(2800)	(-0.4)

Subsequent to the performance of the analyses at liftoff, two structural modes for the after SRB separation event were also selected for use in stability analyses at this latter flight time. These modes and their characteristics are given below.

Item \ Mode	A1	A46
f_n(Hz)	2.3	27.0
G_e (10^{-6}/kg)	7.4	194
(10^{-4} in./lb-sec^2)	(13)	(340)
$\mathscr{P}_n/\phi_e$ (Ns^2/m^3)	464	-0.014
(10^{-5} lb-sec^2/in.^{3})	(-170)	(-0.005)

3.1.3 Stability Results

3.1.3.1 Orbiter End-Burn

The stability results obtained for the basic system at the orbiter end-burn conditions are presented in figure 9. The calculated system critical damping ratios are shown as functions of the assumed structural natural frequency when toleranced ±15 percent. Recalling that the damping of the structural mode is input at 1 percent of critical, it is seen that the damping in the first and second structural modes (f ~ 3 Hz and 5 Hz, respectively) is relatively unaffected by the action of the propulsion system. The seventh and thirtieth modes (f ~ 8 Hz and 22 Hz, respectively) show a somewhat greater effect; however, the minimum value of the calculated damping ratios remains above 0.007. The thirty-fourth mode (f ~ 27 Hz) is strongly affected with the minimum damping ratio being less than 0.002 while the thirty-fifth mode (f ~ 27 Hz) is the worst case with instability being predicted if the structural mode frequency lies within the range 23 to 25 Hz. The damping ratio in this range reached -0.001.* In this last case, the propulsion-system variables in the unstable mode (fig. 10) contain contributions from the interpump mode (real part of the mode shape) and from the sixth feedline-type mode (imaginary part of the mode shape); however, examination of the energy transfer from the propulsion system to the vehicle structure indicates that the instability is primarily due to the coupling with the interpump mode. Therefore, this instability can be identified as an interpump mode type of instability. It was also found that the destabilizing influence on the thirty-fourth mode was also due to coupling with the interpump mode.

3.1.3.2 Liftoff

The results calculated for the liftoff condition are shown in figure 11. In this case it is found that the fundamental mode (f ~ 2 Hz) is unstable

*If the structural gains given by the modal data had been employed, this mode would have remained stable with a minimum damping ratio of 0.003.

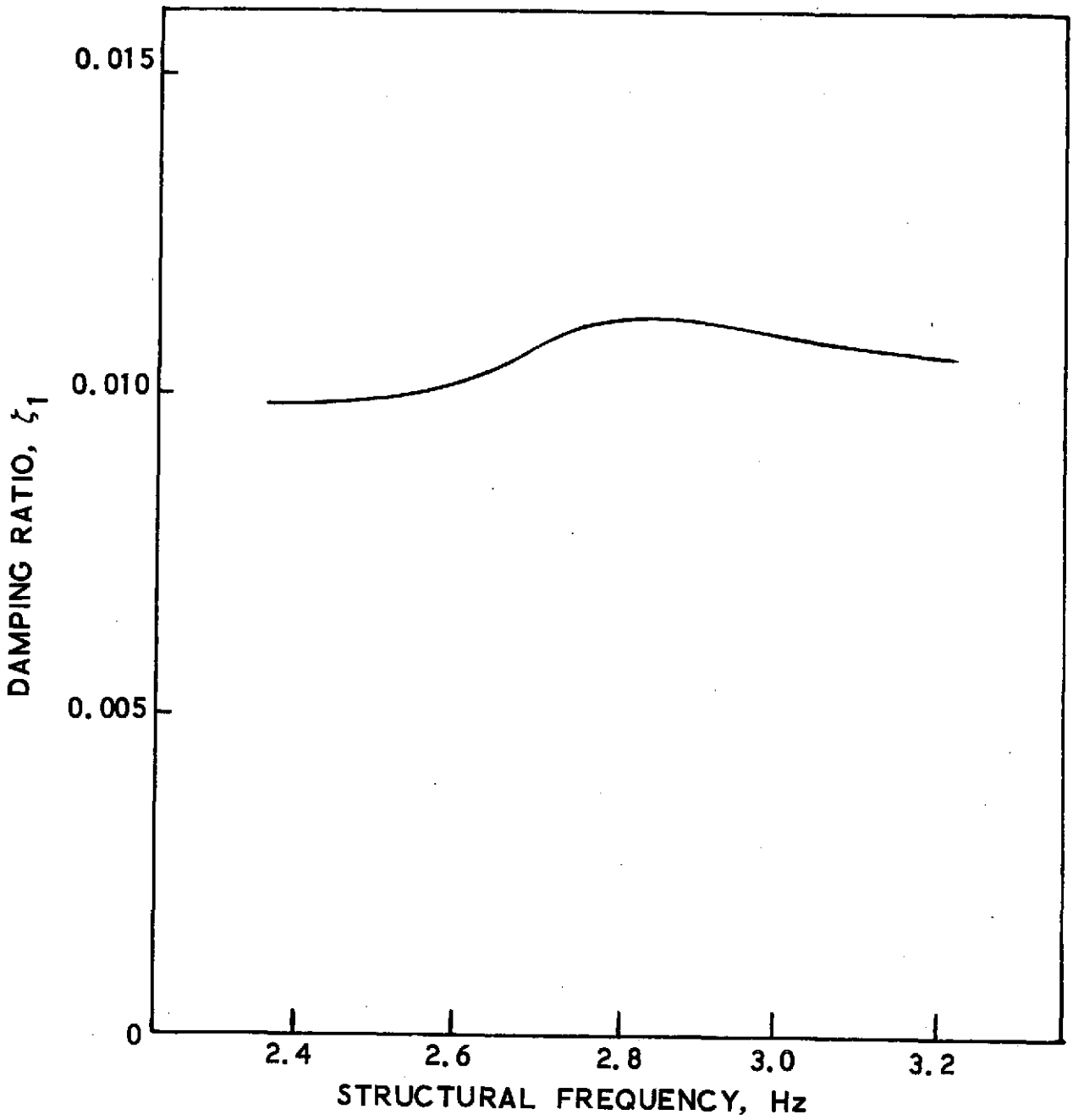

Figure 9a. Stability results for basic system: orbiter end-burn

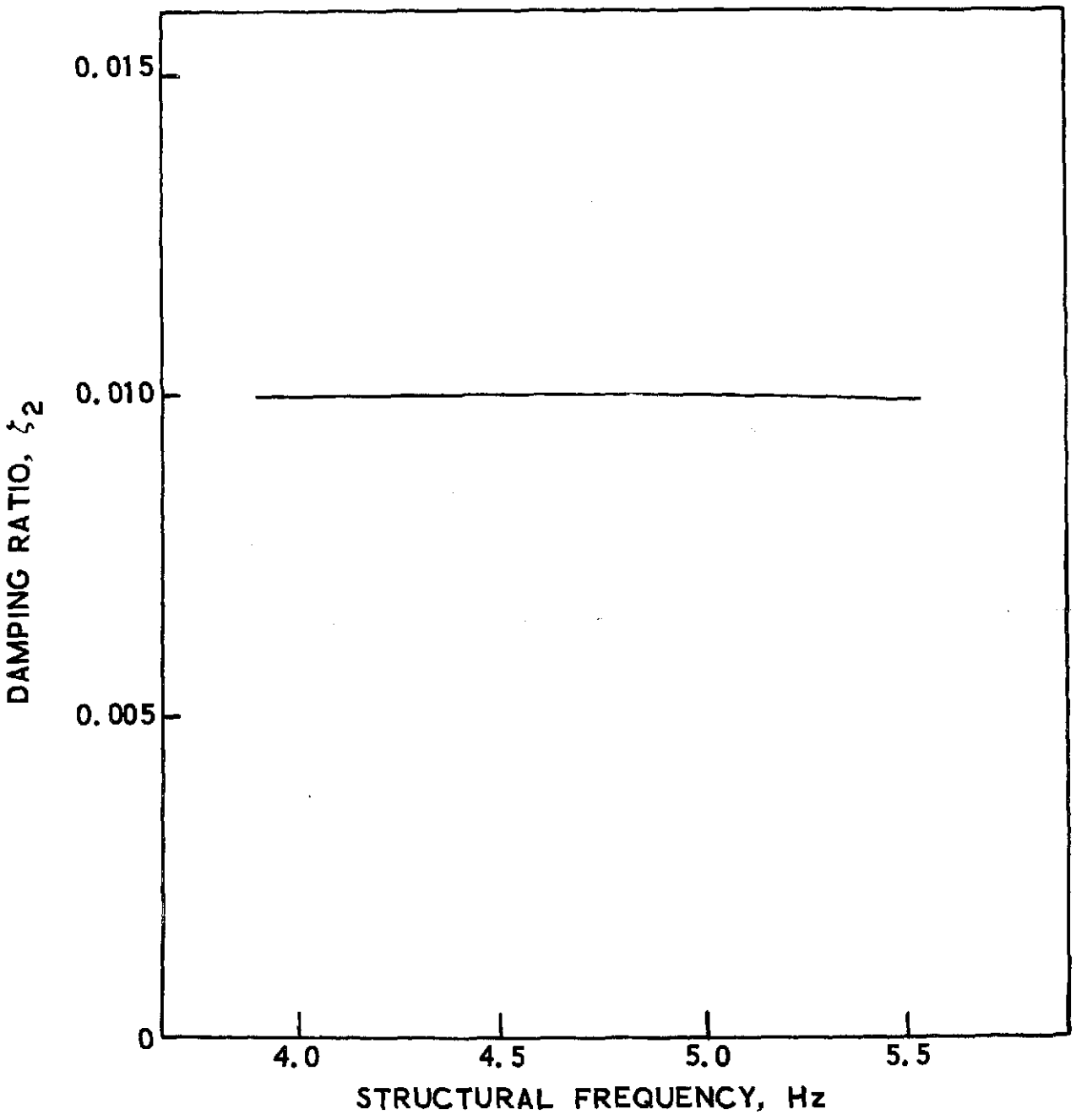

Figure 9b. Stability results for basic system: orbiter end-burn

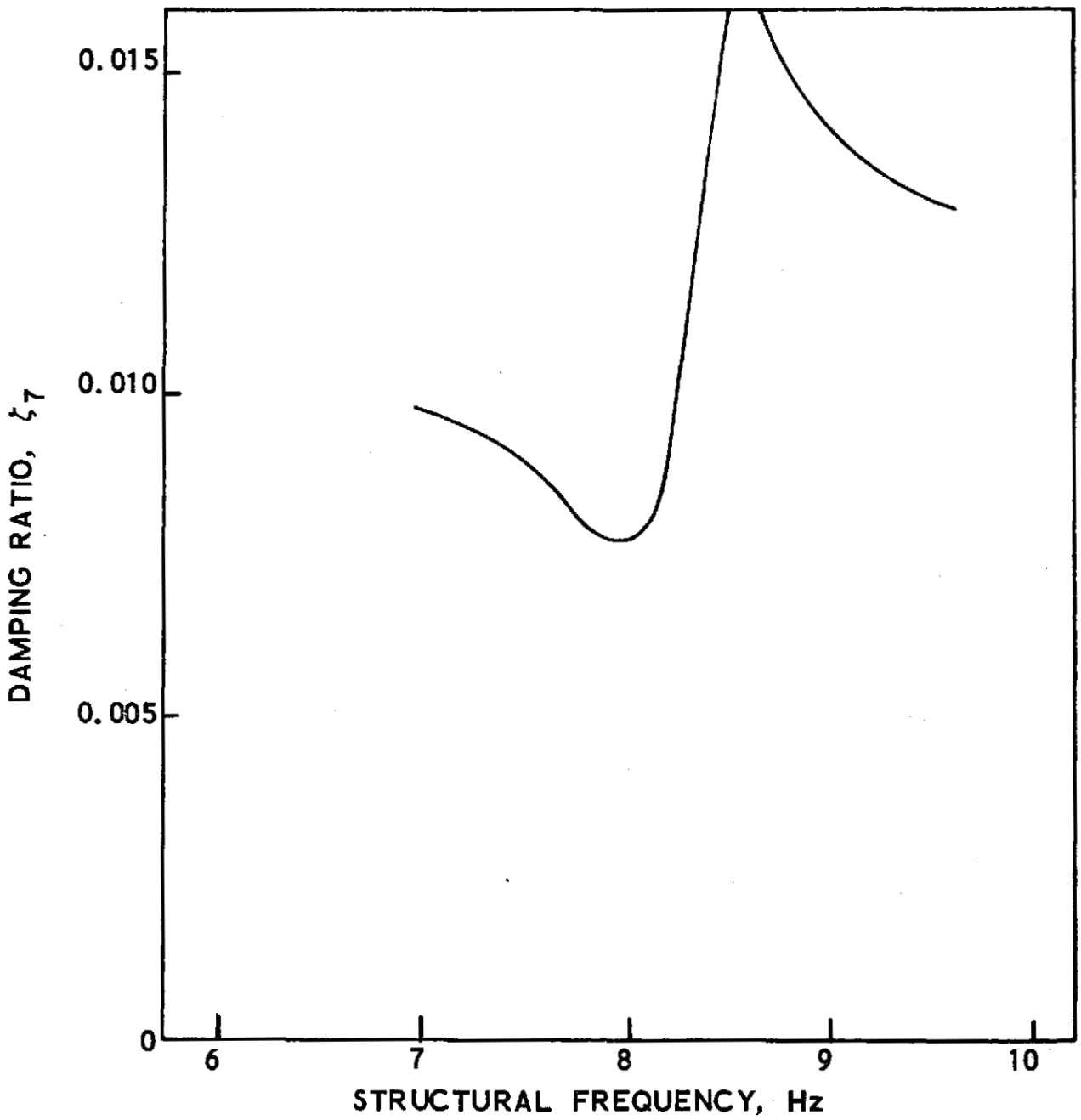

Figure 9c. Stability results for basic system: orbiter end-burn

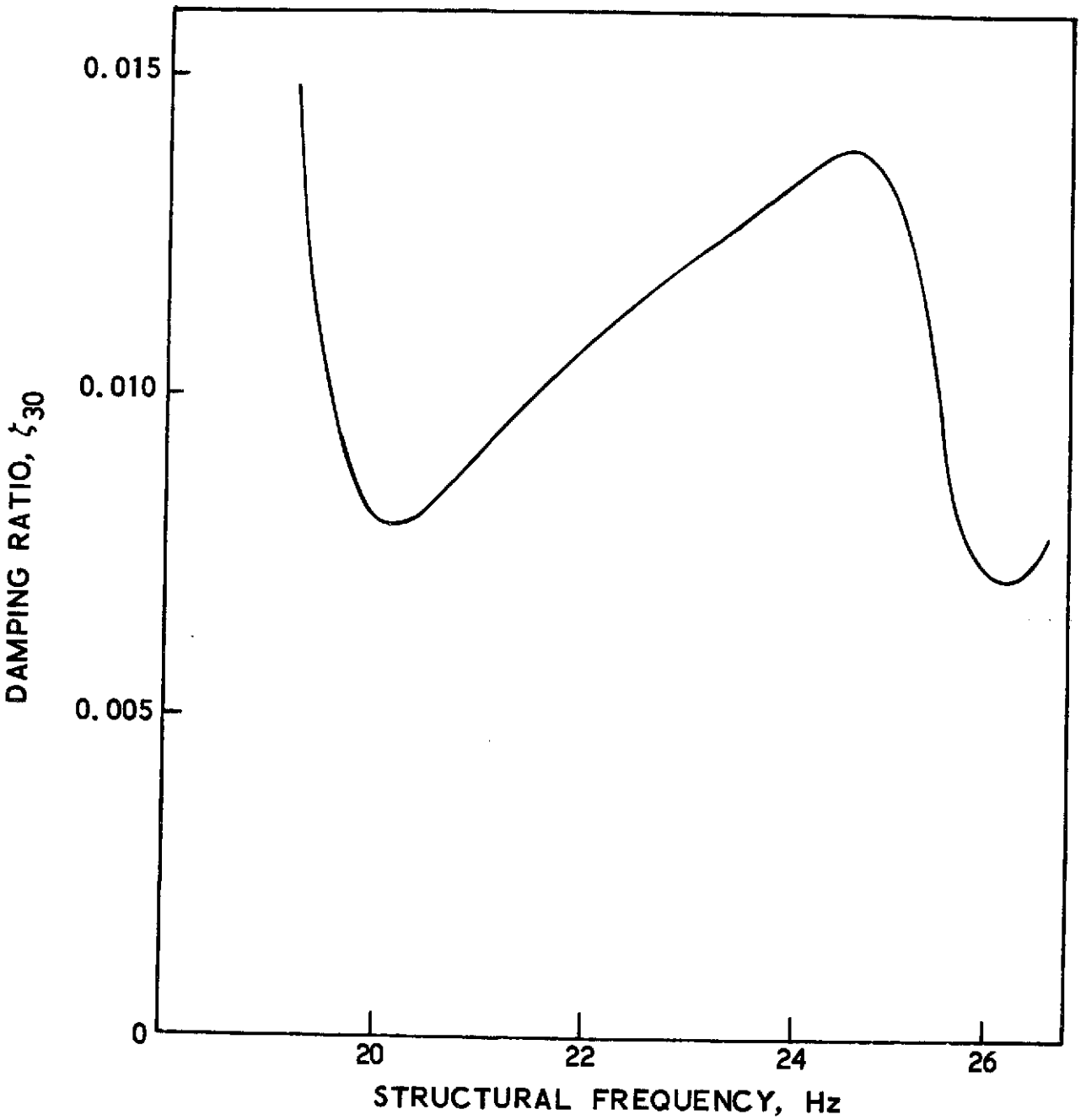

Figure 9d. Stability results for basic system: orbiter end-burn

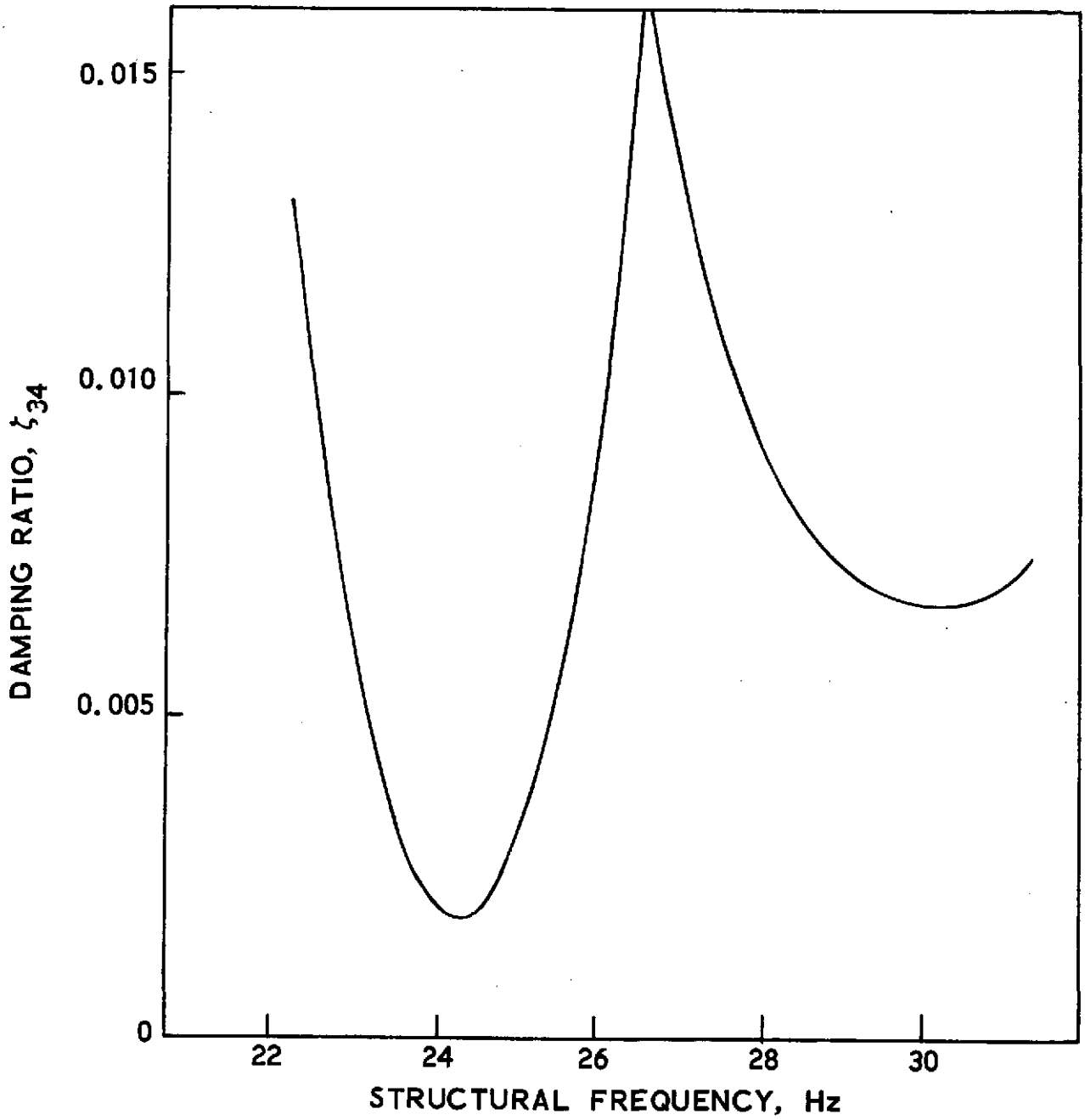

Figure 9e. Stability results for basic system: orbiter end-burn

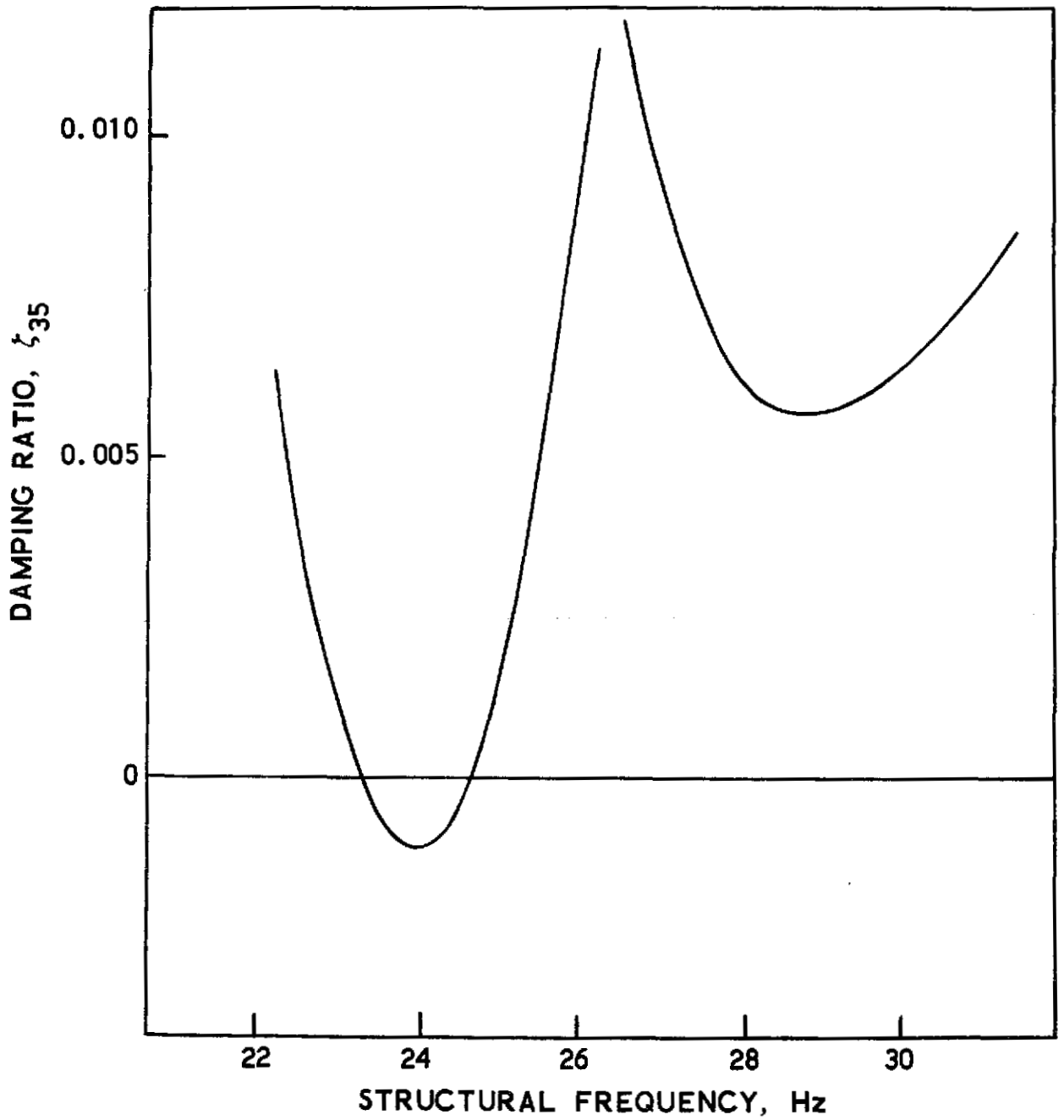

Figure 9f. Stability results for basic system: orbiter end-burn

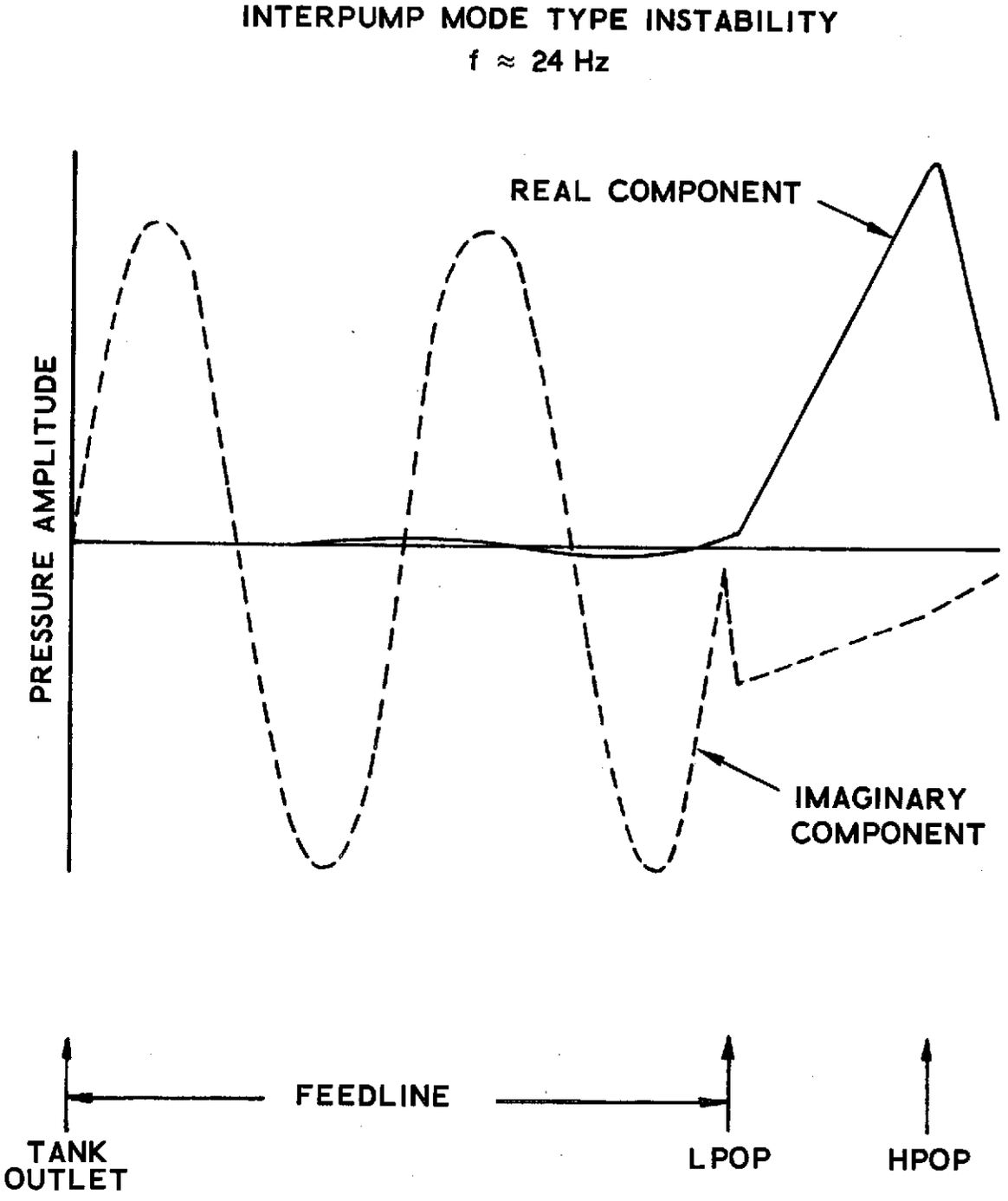

Figure 10. Unstable mode of basic system: orbiter end-burn

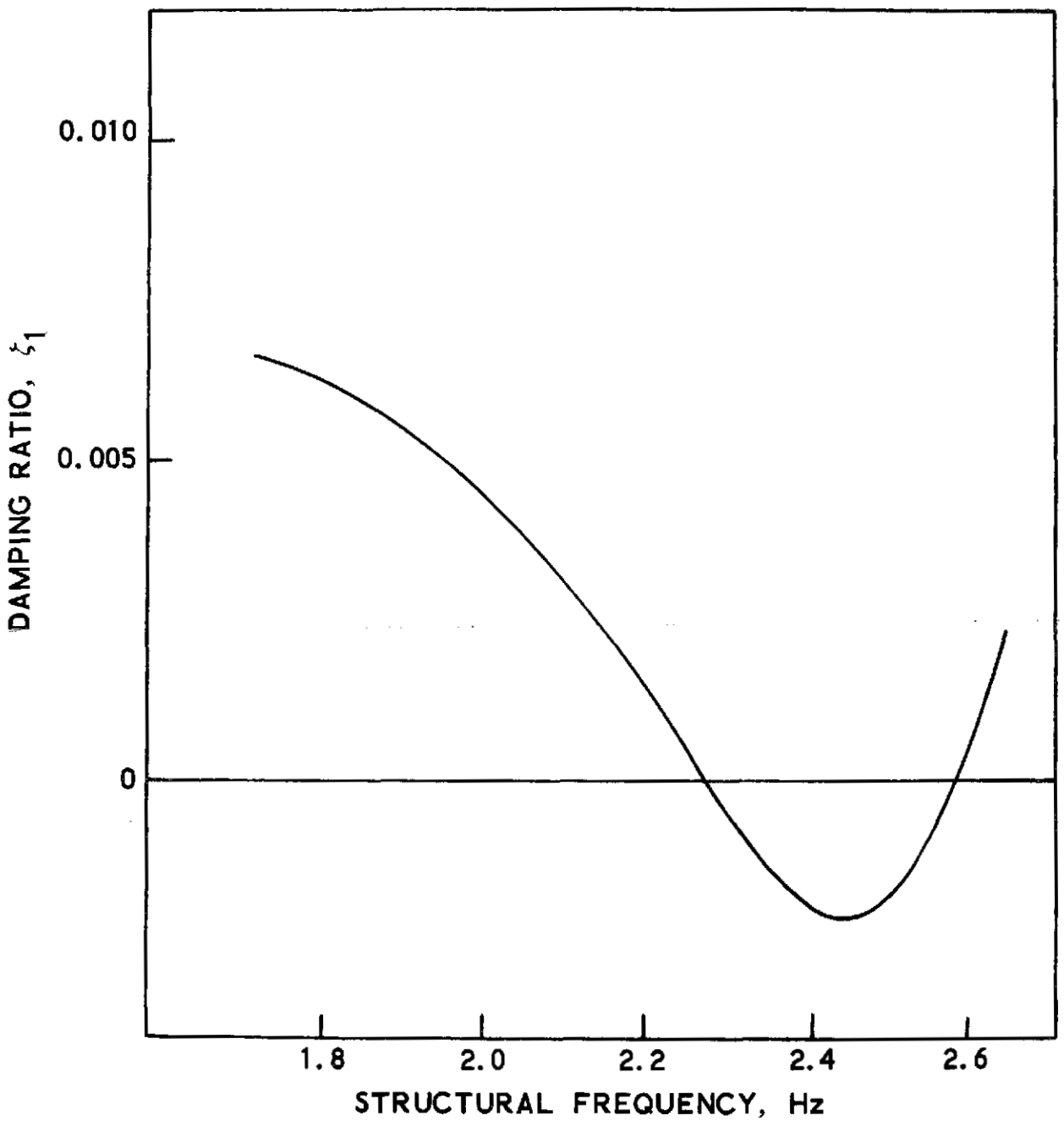

Figure 11a. Stability results for basic system: liftoff

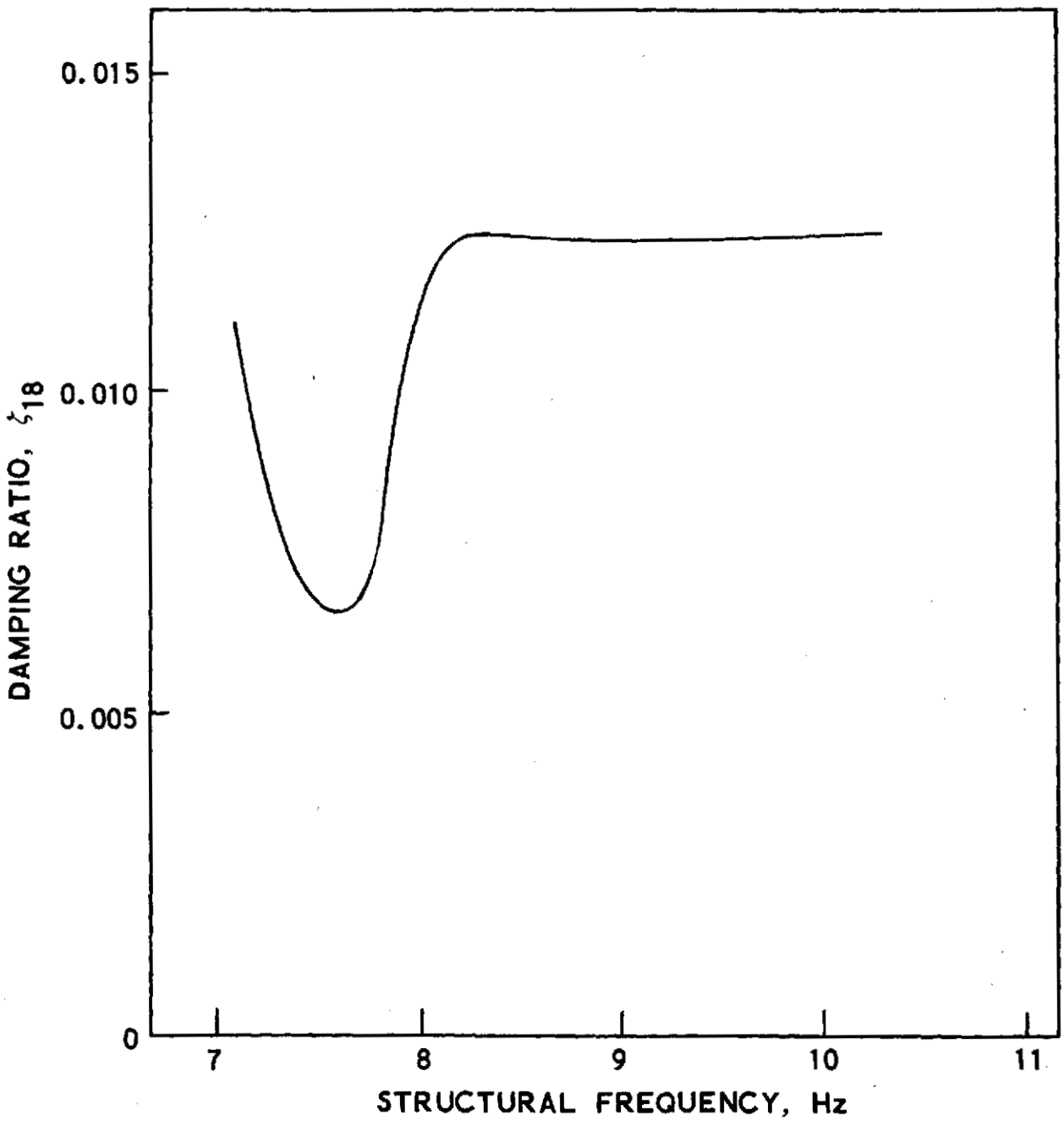

Figure 11b. Stability results for basic system: liftoff

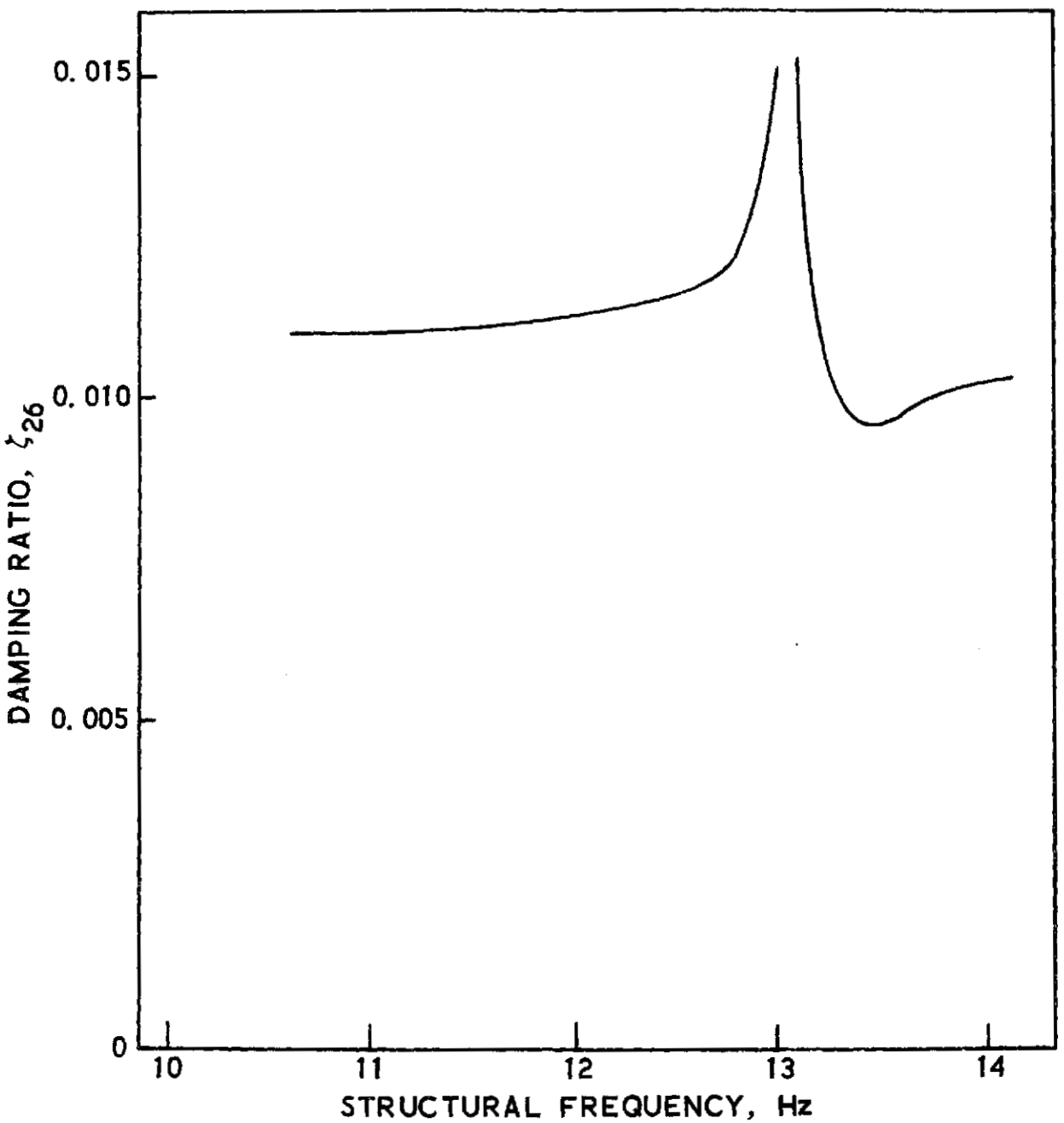

Figure 11c. Stability results for basic system: liftoff

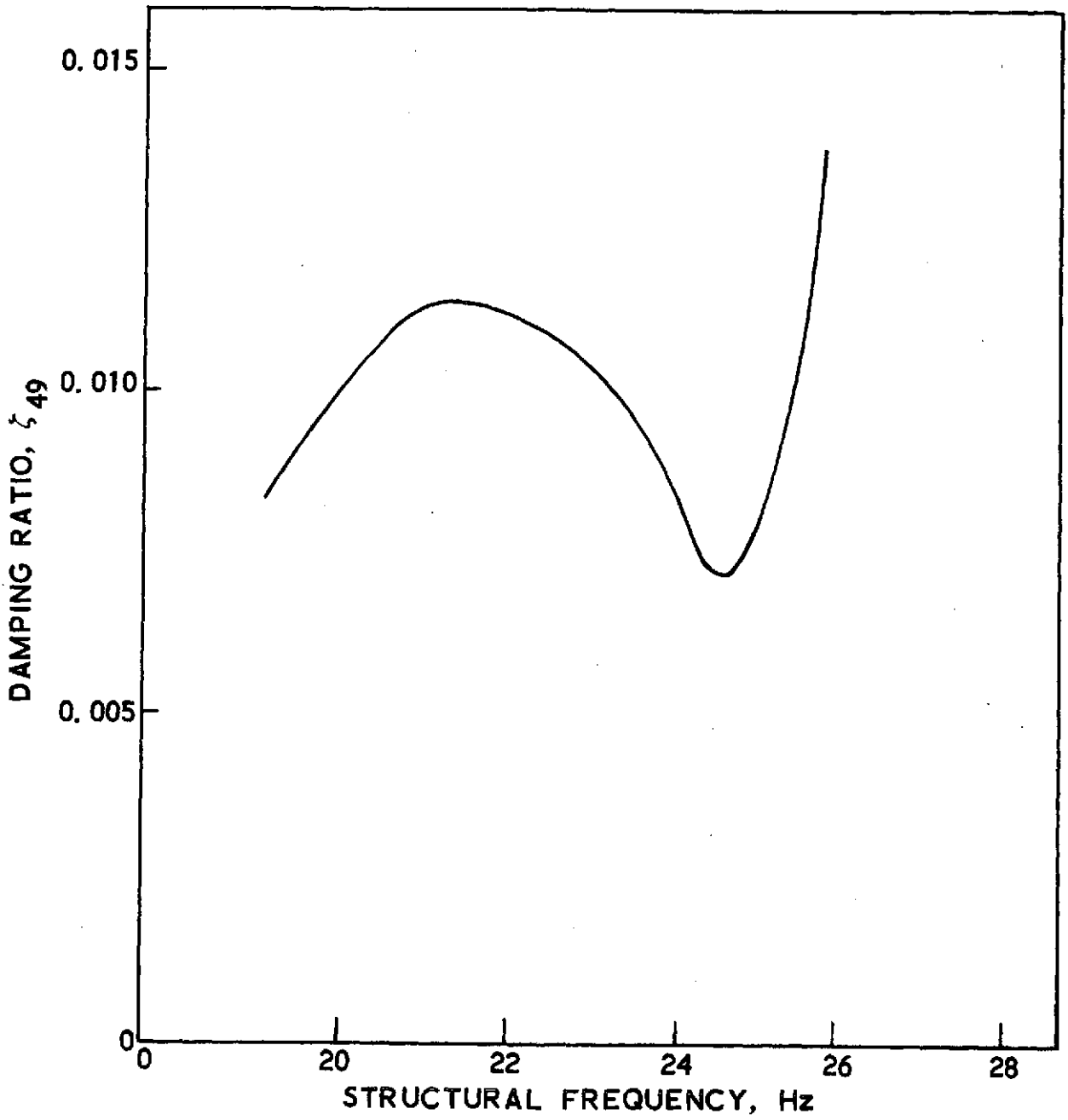

Figure 11d. Stability results for basic system: liftoff

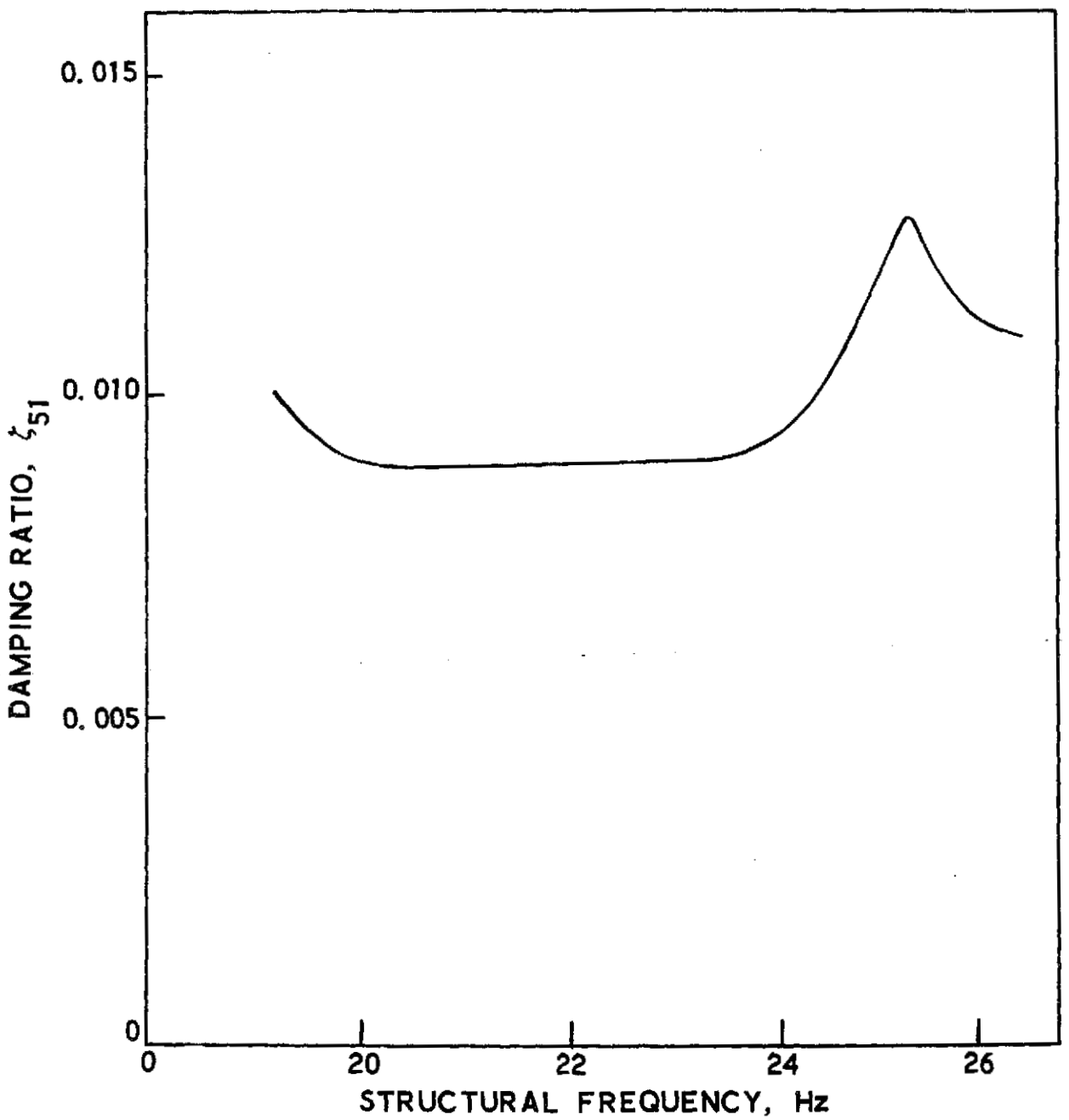

Figure 11e. Stability results for basic system: liftoff

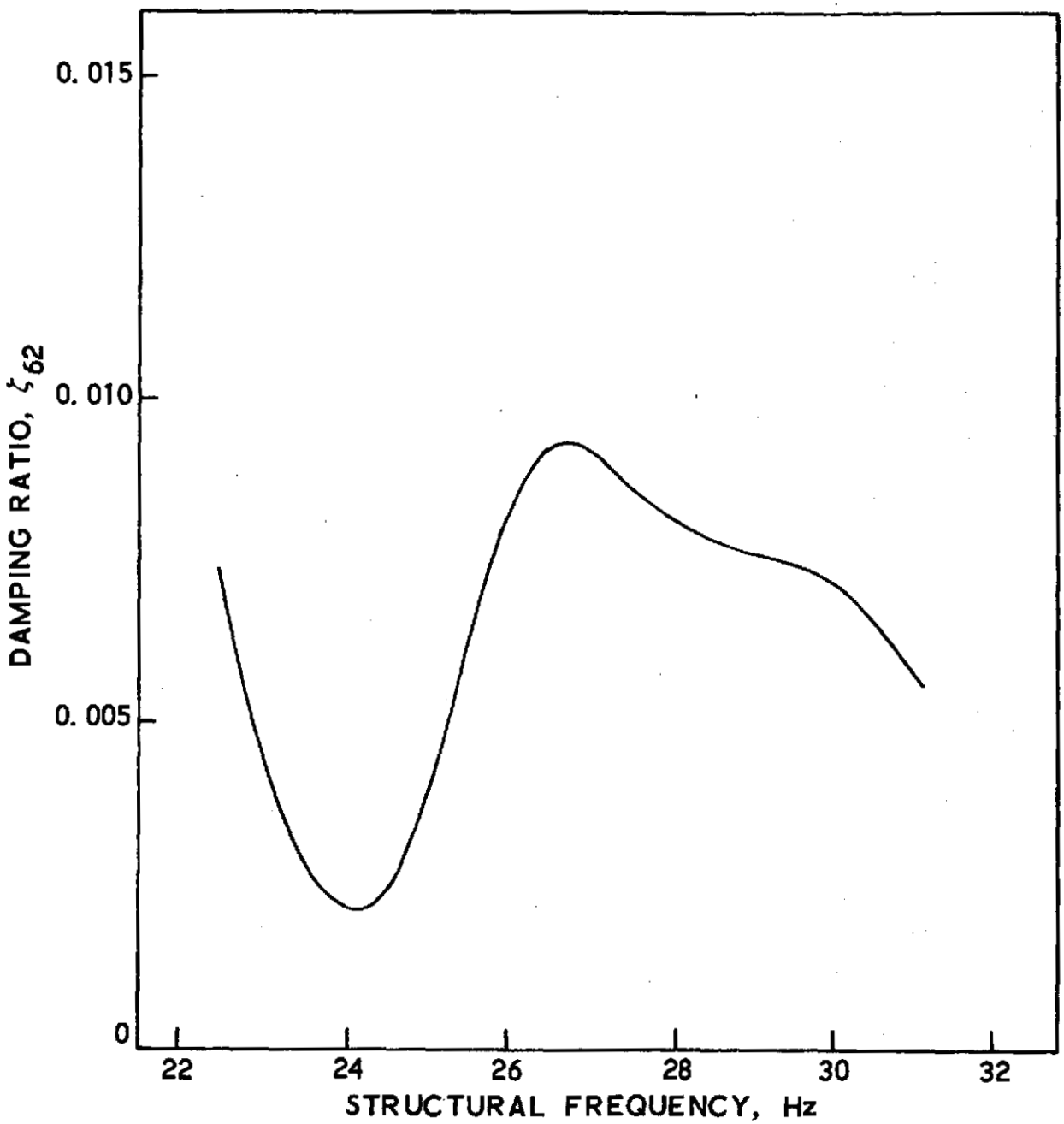

Figure 11f. Stability results for basic system: liftoff

if the first structural-mode frequency lies between about 2.2 to 2.6 Hz; the damping ratio in this range reached -0.002. The other modes are found to be stable. The instability in the fundamental mode results from coupling between the first structural mode and the first feedline-type mode of the propulsion system (fig. 12). The interpump mode primarily couples with the high-gain sixty-second structural mode (f ~ 27 Hz). Although the coupling is significantly destabilizing, it does not produce an instability; the minimum calculated value of the damping ratio in this case being about 0.002.

3.1.3.3 After SRB Separation

The results calculated for this flight condition are shown in figure 13. In this instance the fundamental mode (f ~ 2 Hz) is seen to be unstable over a relatively wide range of the first structural mode frequency (~1.9 Hz to ~2.6 Hz). Again the instability results from coupling between the first feedline-type mode of the propulsion system and the first structural mode. The instability is severe, the damping ratio reaching about -0.009. The high gain forty-sixth structural mode (f ~ 27 Hz) remains stable but loses a good deal of damping in the 22 to 26 Hz frequency range due to destabilizing coupling with the interpump mode; the minimum calculated value of the damping ratio in this instance being about 0.003.

3.2 System with Compliant Accumulator

The effect on the system stability characteristics of the introduction of a compliant accumulator are now examined. The employed accumulator has a 0.057 m^3 (2 ft^3) volume and is located at either the LPOP inlet, the LPOP discharge, or the HPOP inlet.

3.2.1 Propulsion-System Modes

The introduction of the compliant accumulator into the propulsion system generally produced shifts of the feedline-type mode frequencies that were within the associated open-open and open-closed feedline frequency bands. The frequency of the interpump mode was not significantly changed by the presence of accumulators at either the LPOP inlet or at the LPOP discharge. However, the presence of an accumulator at the HPOP inlet reduced this frequency appreciably. For example, at the end-burn and liftoff conditions the reductions were from 24.4 to 14.9 Hz and from 23.1 to 9.45 Hz, respectively.

3.2.2 Selection of Cases

With the exception of the end-burn condition, the same set of structural modes was used as was employed previously in the analysis of the basic system. The exception at end-burn was the introduction of the twenty-first structural mode into the analysis for the accumulator at the HPOP-inlet location. This mode had a frequency of 15.9 Hz and was introduced since it could possibly couple with the 14.9-Hz interpump mode.

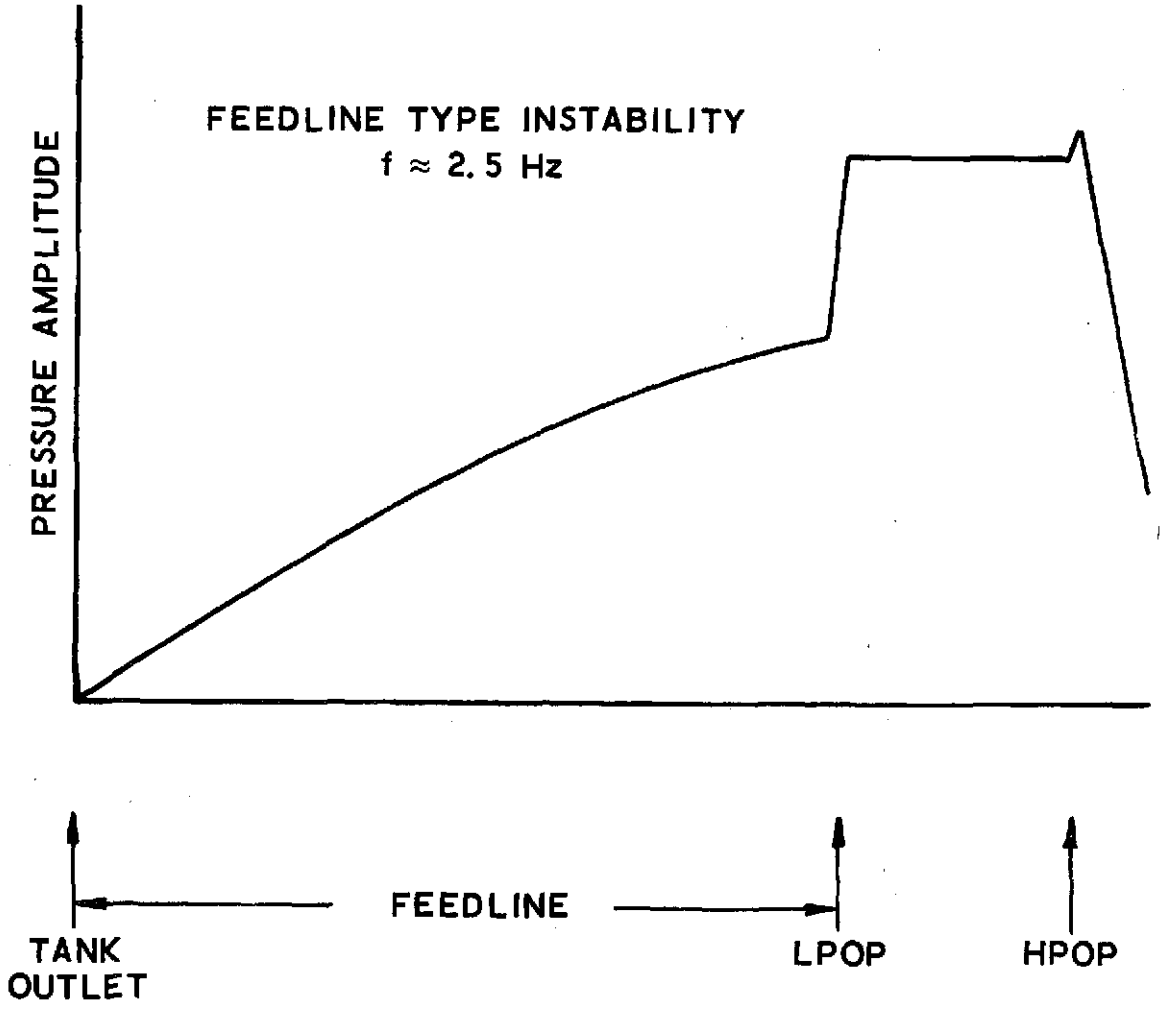

Figure 12. Unstable mode of basic system: liftoff

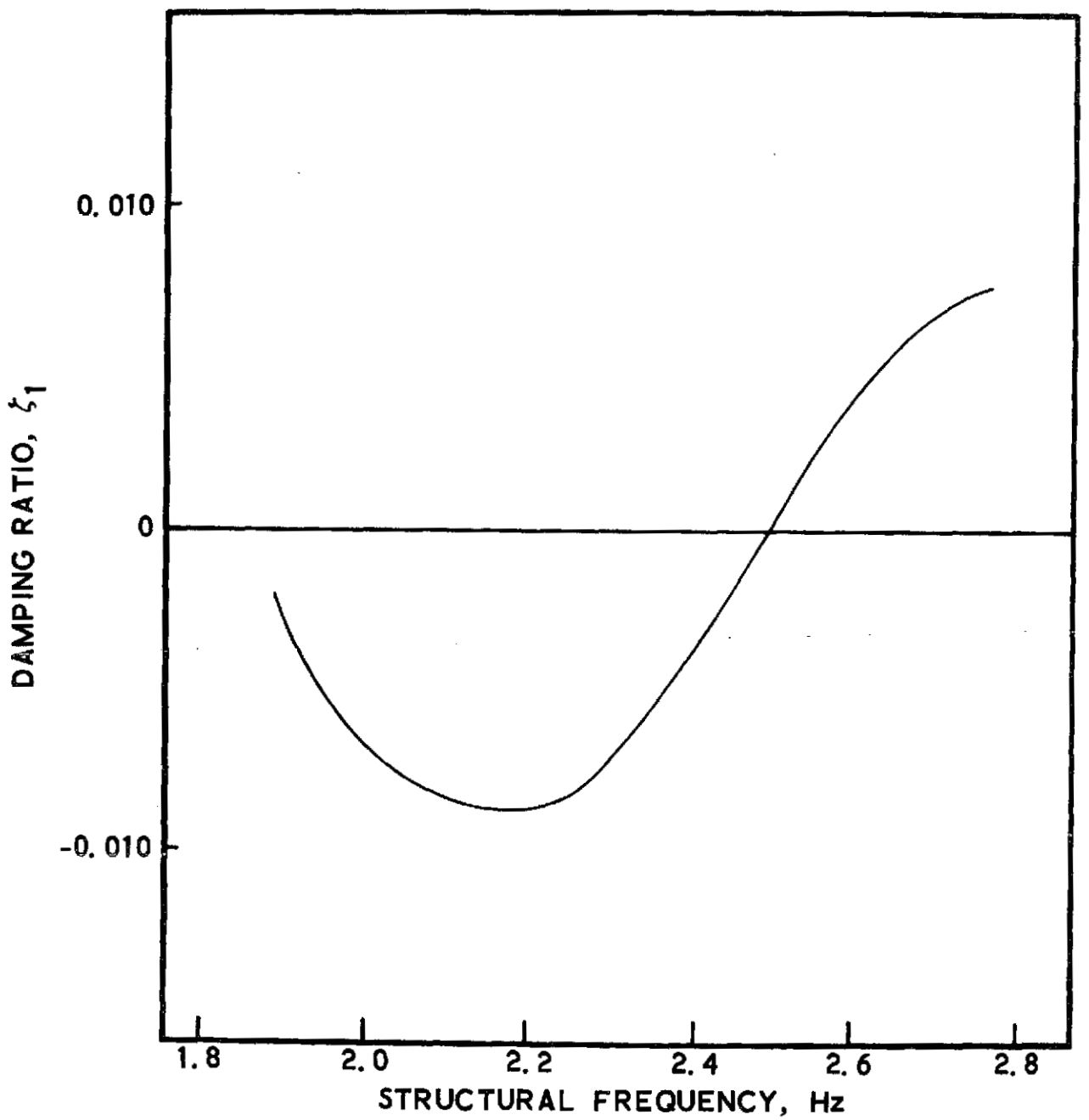

Figure 13a. Stability results for basic system: after SRB separation

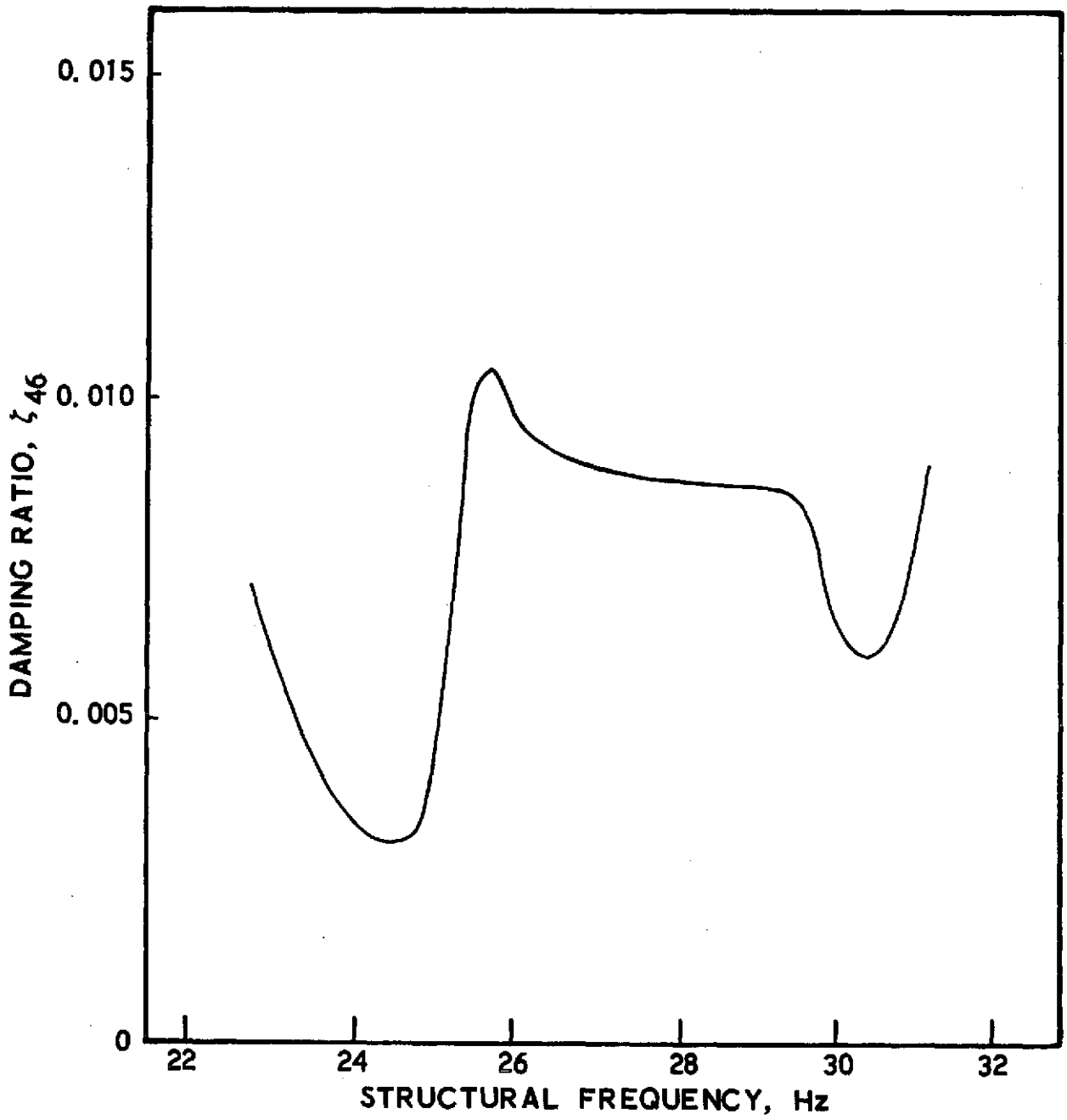

Figure 13b. Stability results for basic system: after SRB separation

3.2.3 Stability Results

3.2.3.1 Orbiter End-Burn

The results calculated for this case indicated that the stability of the lower structural modes used in the analyses (modes E1 through E30) was somewhat enhanced by the presence of the compliant accumulators at any of the three positions; the minimum value of the damping ratio calculated for these modes being in excess of 0.0085. However, the case for the two proximate high-gain modes, the thirty-fourth and thirty-fifth modes, was radically different. The results for the thirty-fourth mode, shown in figure 14a, reveal that the introduction of a compliant accumulator at the LPOP discharge renders the system unstable for structural mode frequencies in the range 22.5 to 24.6 Hz. The introduction of an accumulator at the LPOP inlet produces a decrease in damping with decrease in the structural mode frequency. The system does not become unstable, however, within the specified range of structural frequencies. In contrast to these results, an accumulator at the HPOP inlet is relatively beneficial. Similar trends are observed in the case of the thirty-fifth mode (fig. 14b). It is seen that the introduction of an accumulator at either the LPOP discharge or at the LPOP inlet intensified the instability that was previously predicted for the basic system.* The intensification is particularly severe for the LPOP discharge case where the minimum calculated damping ratio drops to about -0.010 as compared to the worst case value of around -0.001 for the basic system. In view of the poor showing of the LPOP-discharge accumulator at this end-burn condition, it was decided to drop this location from the subsequent analyses. Unlike the two LPOP locations, the introduction of an accumulator at the HPOP inlet is seen to be beneficial. The instability is eliminated and the minimum damping ratio maintained above 0.006 over the specified range of structural frequencies. The pronounced effectiveness of the HPOP-inlet accumulator in the case of these two modes is undoubtedly due to the lowering of the interpump mode resonant frequency. The stability analyses indicated that the introduction of possible coupling between the interpump mode (of the system with the HPOP-inlet accumulator) and the twenty-first structural mode was not significant - probably due to lower structural gain in this mode (about 2.5×10^{-5} l/kg).

From practical consideration on the size of the accumulator, it is of some interest to see if the effectiveness of an accumulator at the HPOP inlet would be degraded by a reduction in the accumulator volume from the original 0.057-m^3 (2 ft^3) value. This was checked by performing calculations for the thirty-fifth mode using a 0.029-m^3 (1 ft^3) volume accumulator and a 0.014-m^3 (0.5 ft^3) volume accumulator. The results calculated for these designs are shown in figure 15, where it is seen that the specified reductions in volume did not degrade the performance of the accumulator insofar as suppression of the interpump mode instability was concerned.

Finally, it might be argued that the failure of the LPOP-inlet accumulator to eliminate the instability in the high gain thirty-fifth structural mode was due to an inadequate level of compliance. To check this supposition, an additional stability analyses was undertaken for this mode assuming a

*If the structural gain given by the modal data had been employed for the thirty-fifth mode, the system would have remained stable with the LPOP inlet accumulator and would have become unstable with the LPOP discharge accumulator. In the former case the introduction of the accumulator was destabilizing in that the minimum damping ratio of the system was reduced.

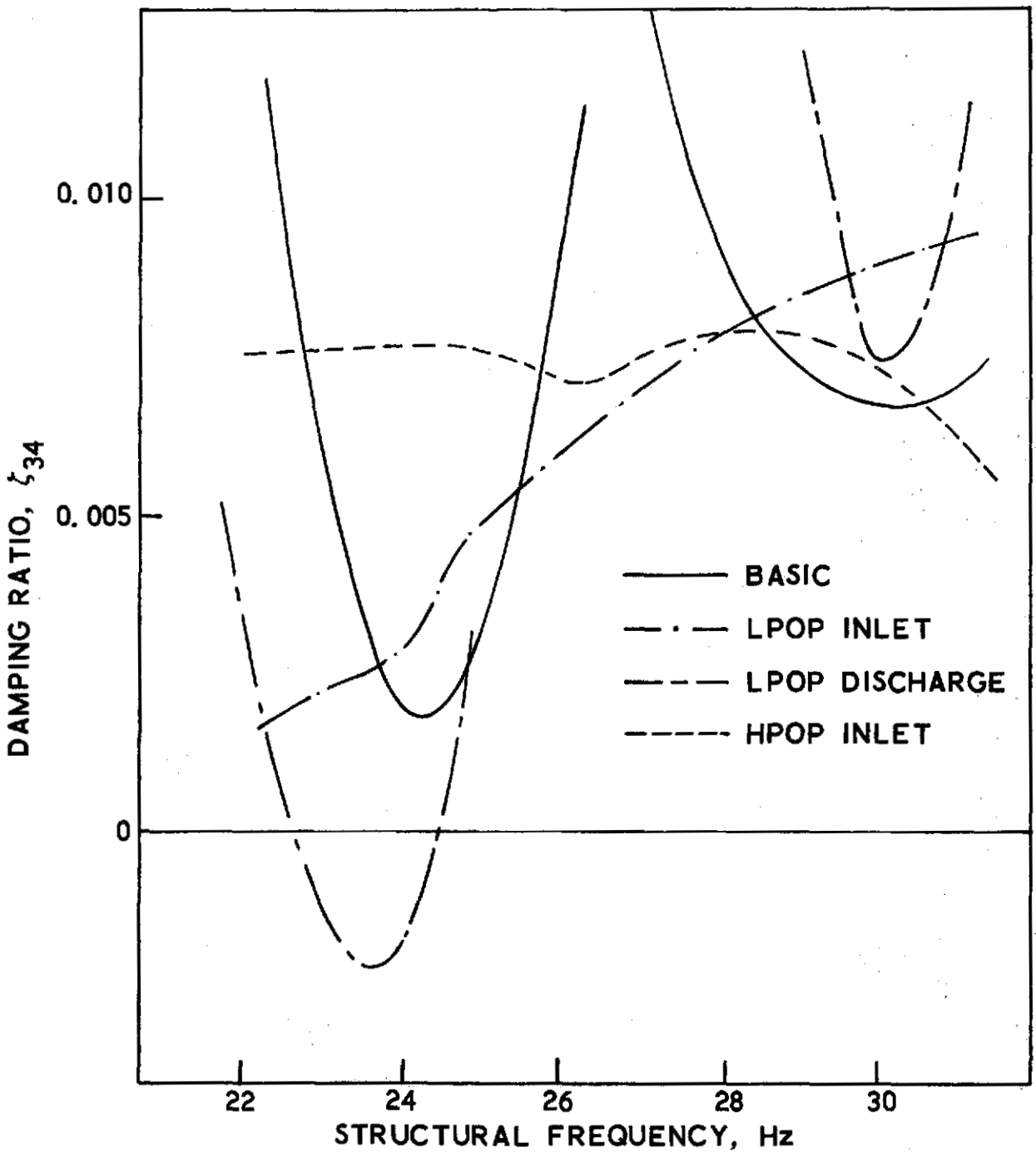

Figure 14a. Stability results with compliant accumulator: orbiter end-burn

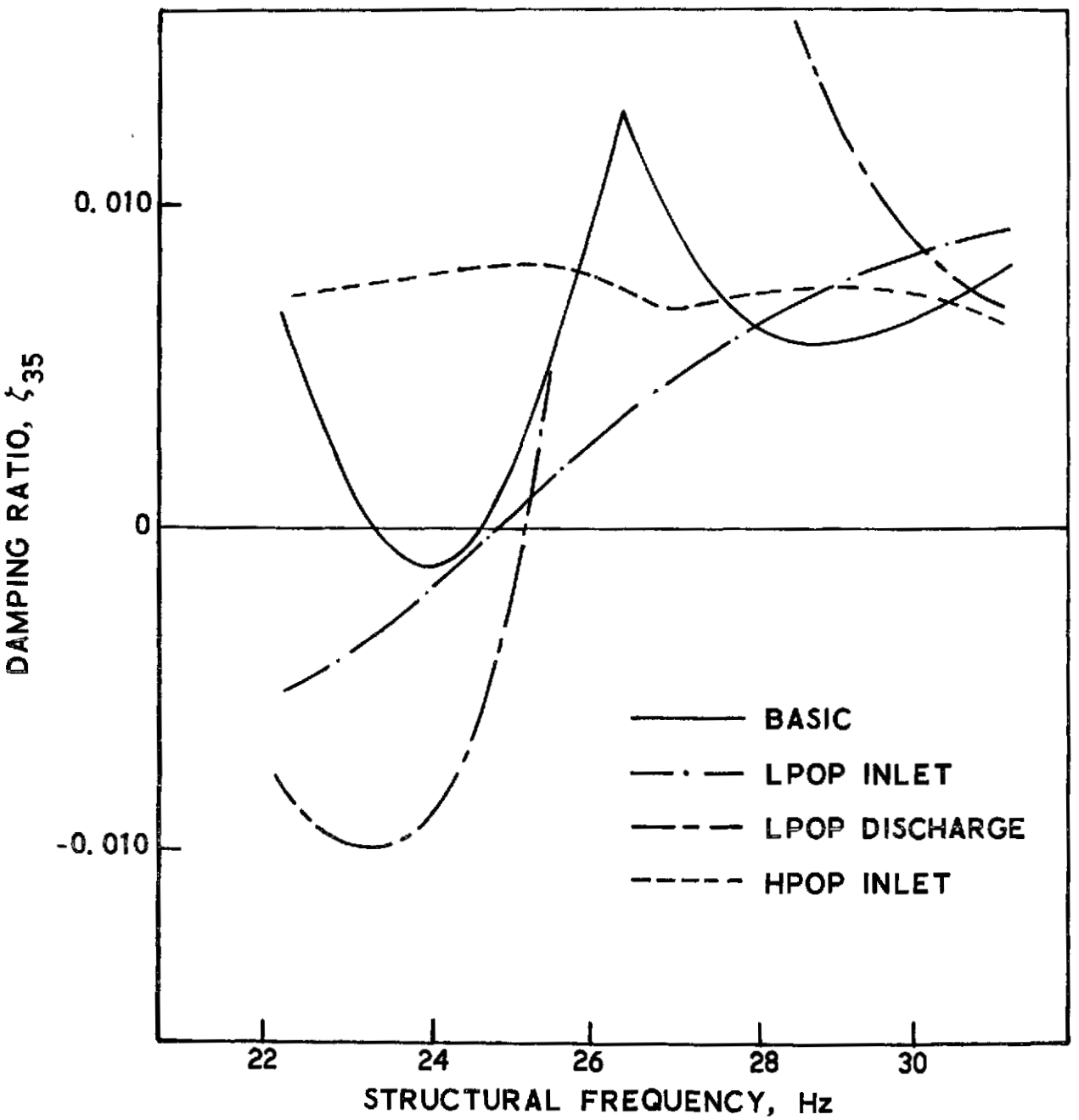

Figure 14b. Stability results with compliant accumulator: orbiter end-burn

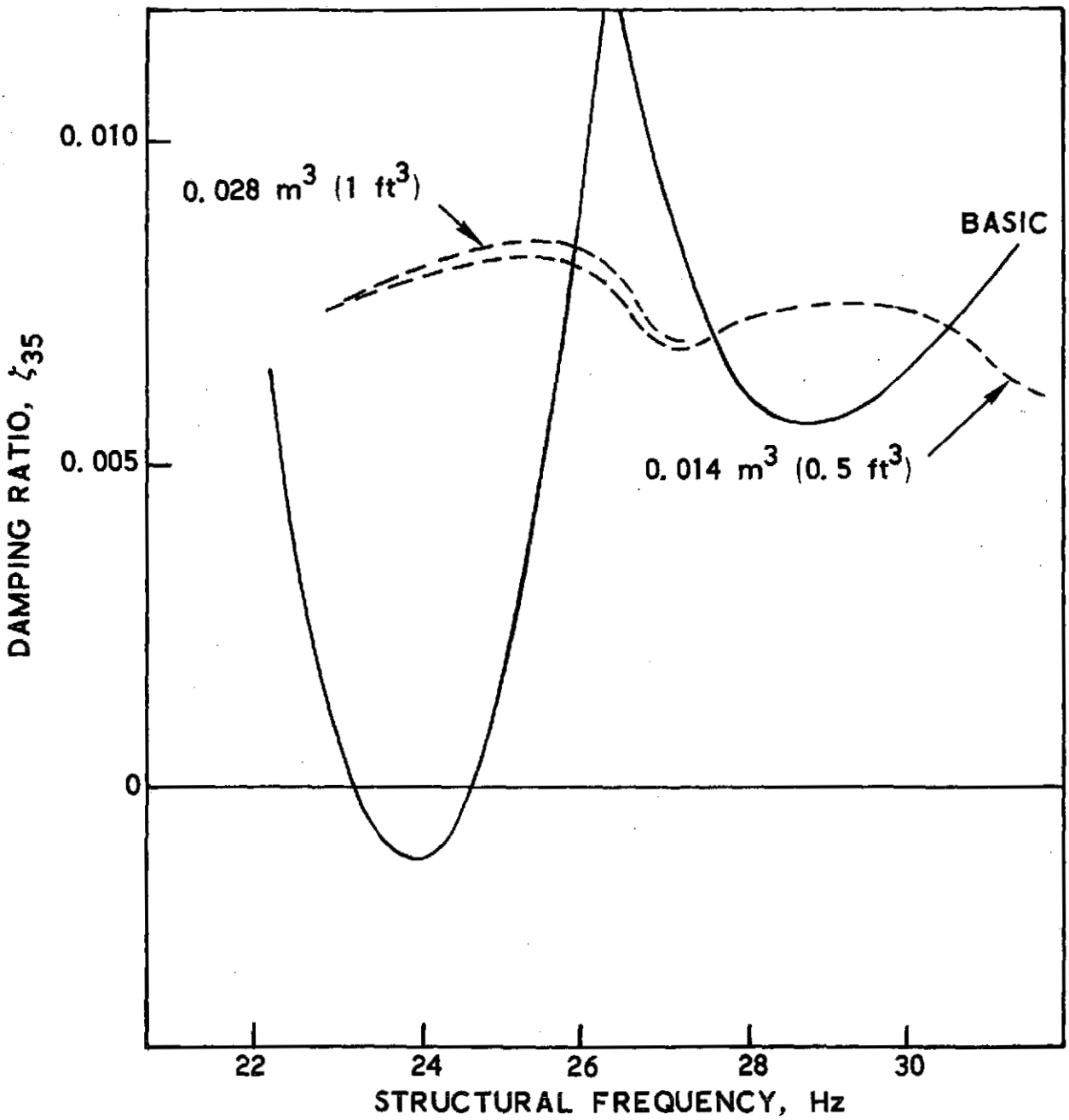

Figure 15. Variation of stability with compliant accumulator volume for HPOP inlet location: orbiter end-burn

0.57-m^3 (20 ft^3) volume accumulator at the LPOP inlet. This accumulator volume change produced a ten-fold increase in the accumulator compliance. The resulting stability results were essentially identical to those obtained for the 0.057-m^3 (2 ft^3) accumulator thereby indicating that the inadequacy of the LPOP-inlet suppressor lay with its location rather than in its size.

3.2.3.2 Liftoff

The results calculated for the liftoff condition indicated that the introduction of an accumulator at either the LPOP inlet or the HPOP inlet would eliminate the instability previously predicted in the fundamental mode (fig. 16). The effectiveness of the LPOP-inlet accumulator in this case is attributed to the fact that the fundamental mode instability at liftoff involves coupling between a structural mode and the fundamental feedline-type mode of the propulsion system (unlike the end-burn instability that involves the interpump mode of the propulsion system). It is also interesting to note that the HPOP-inlet accumulator, which was effective in eliminating the interpump mode type of instability at end-burn, is also effective in eliminating the feedline-type instability at liftoff. As was done at the end-burn condition, the change in the effectiveness of the accumulator at the HPOP inlet with decrease of the accumulator volume to 0.029 m^3 (1 ft^3) and 0.014 m^3 (0.5 ft^3) was checked. The results in this case (fig. 17) were quite different and indicated a sensitivity to accumulator volume over the variation that was considered. In the case of the 0.029-m^3 (1 ft^3) accumulator, the minimum value of the damping ratio was reduced to 0.009 (from about 0.013 for the 0.057 m^3 accumulator). In the case of the 0.014-m^3 (0.5 ft^3) accumulator, the minimum damping value became negative at the lower end of the structural frequency range. Thus, an accumulator of this size did not eliminate the feedline-type mode instability. This failure is attributed to an insufficient lowering of the frequency of the fundamental propulsion-system mode.

With regard to the effect of the 0.057-m^3 (2 ft^3) accumulator on the higher structural modes, some destabilizing influences on the fifty-first mode ($f \sim 22$ Hz) were found with the introduction of an accumulator at either the LPOP inlet or the HPOP inlet (fig. 18a). The mode remained stable in both cases, however, maintaining damping ratios in excess of 0.005. A destabilizing influence of the LPOP inlet accumulator was exhibited with the sixty-second mode ($f \sim 27$ Hz); the system barely remaining stable at the lower end of the frequency range of interest (fig. 18b). In contrast, the HPOP inlet accumulator had a beneficial effect on this mode increasing the minimum damping ratio from around 0.002 for the basic system up to about 0.006.

3.2.3.3 After SRB Separation

As in the liftoff case, it was found that an accumulator at either the LPOP inlet or HPOP inlet will eliminate the fundamental mode instability that had been predicted for the basic system (fig. 19). This was particularly encouraging since the degree of instability in the fundamental mode for this flight condition was considerably more severe than for the liftoff event. A

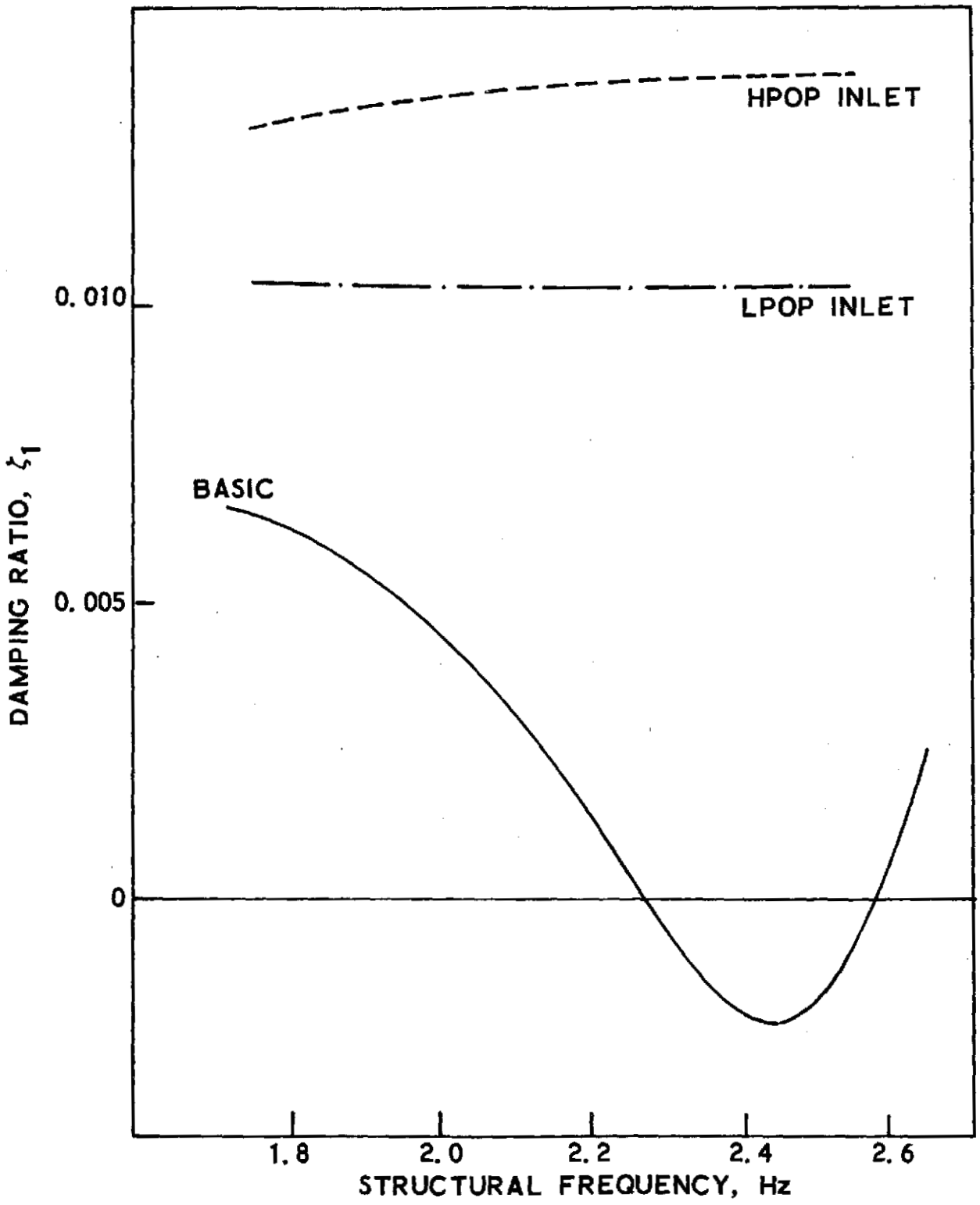

Figure 16. Fundamental mode stability with compliant accumulator: liftoff

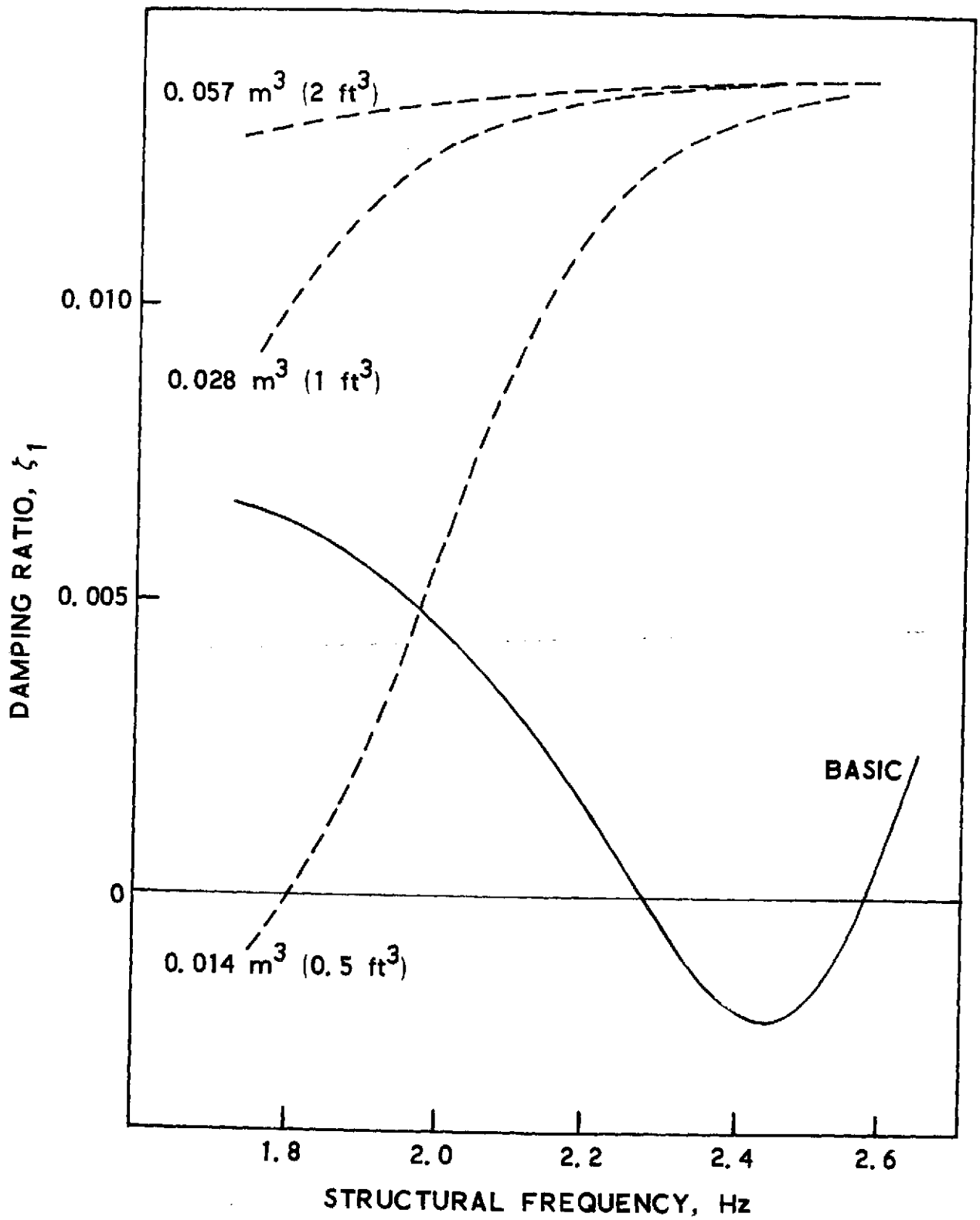

Figure 17. Variation of stability with compliant accumulator volume for HPOP inlet location: liftoff

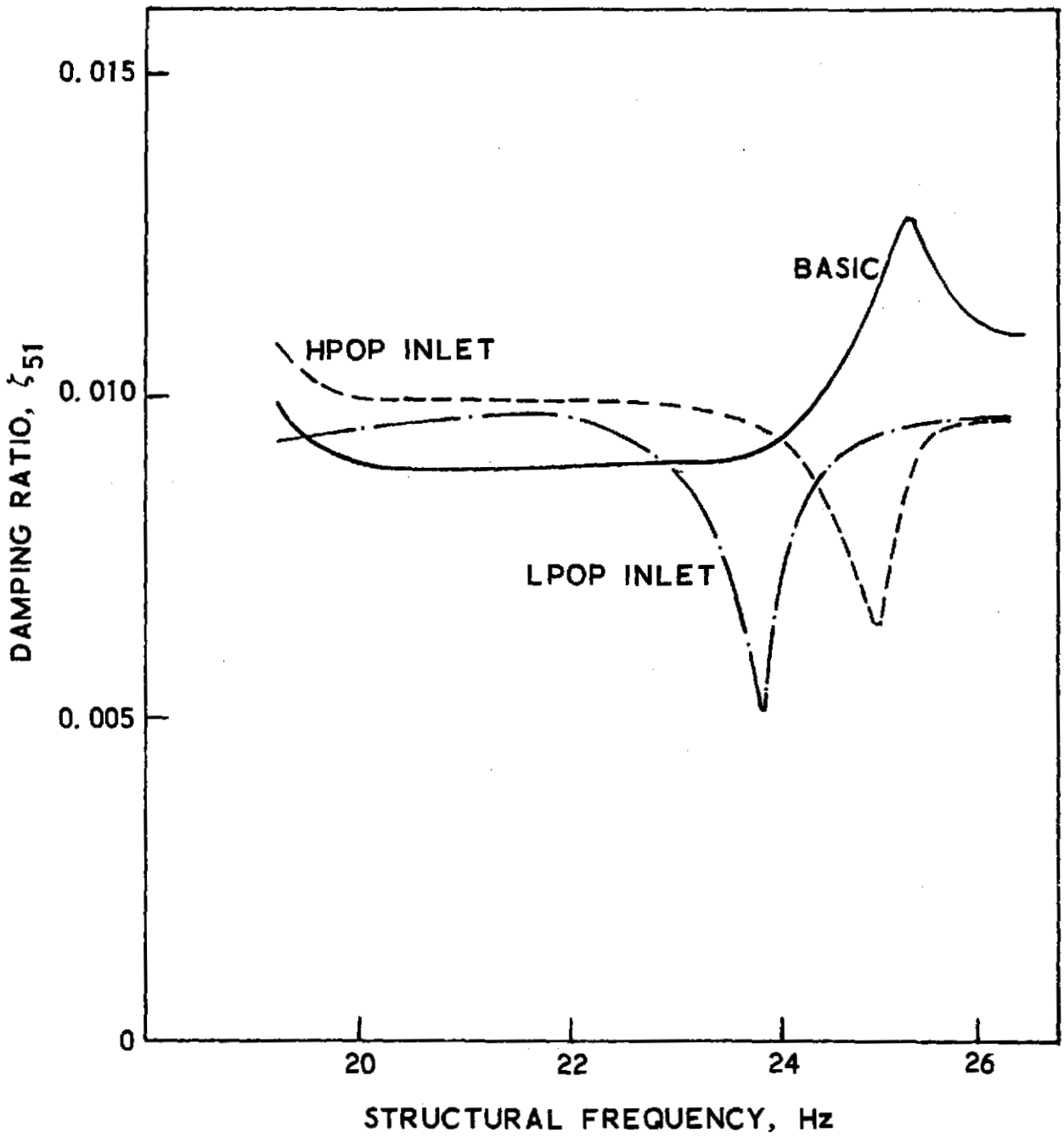

Figure 18a. Stability results with compliant accumulator: liftoff

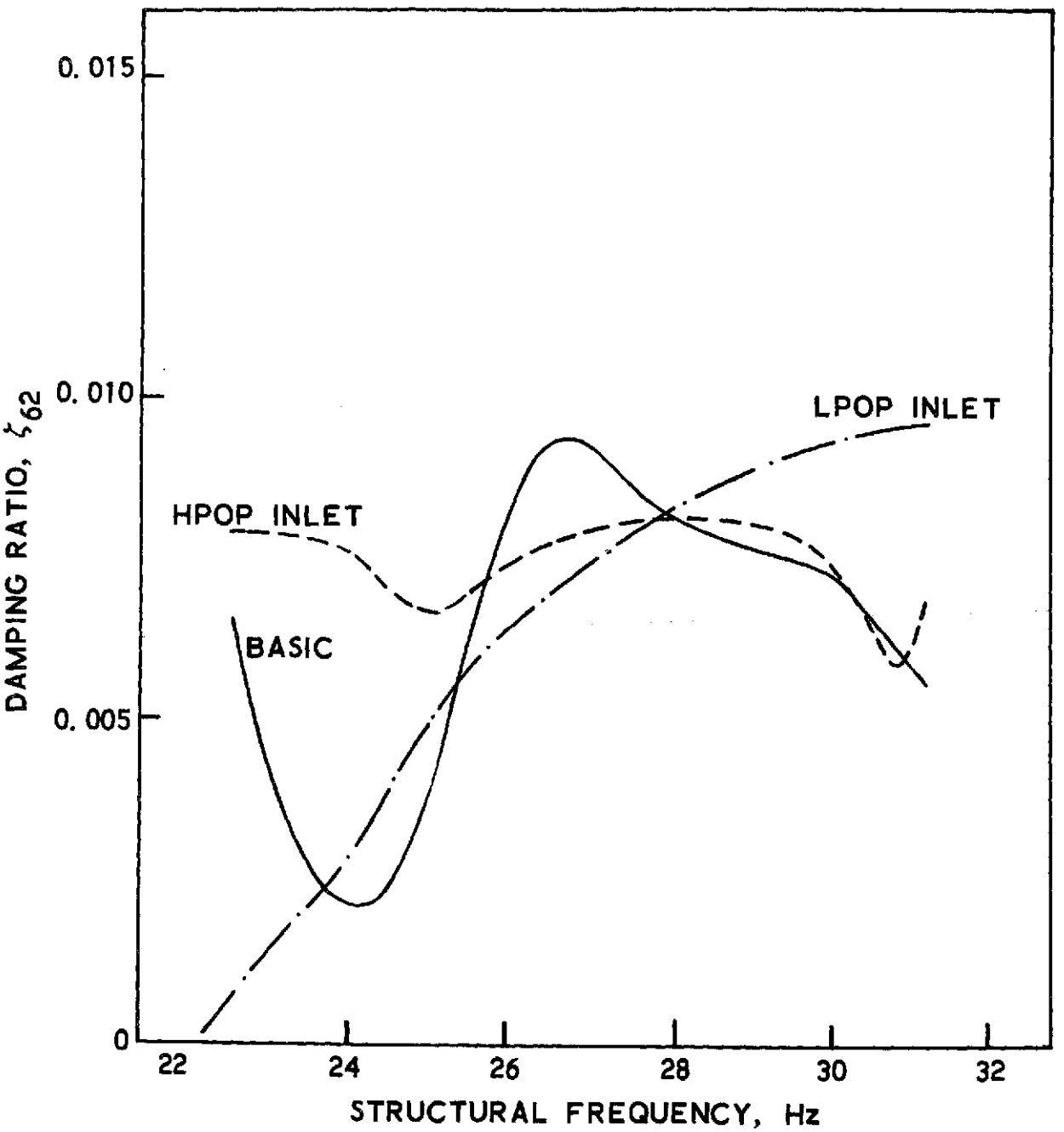

Figure 18b. Stability results with compliant accumulator: liftoff

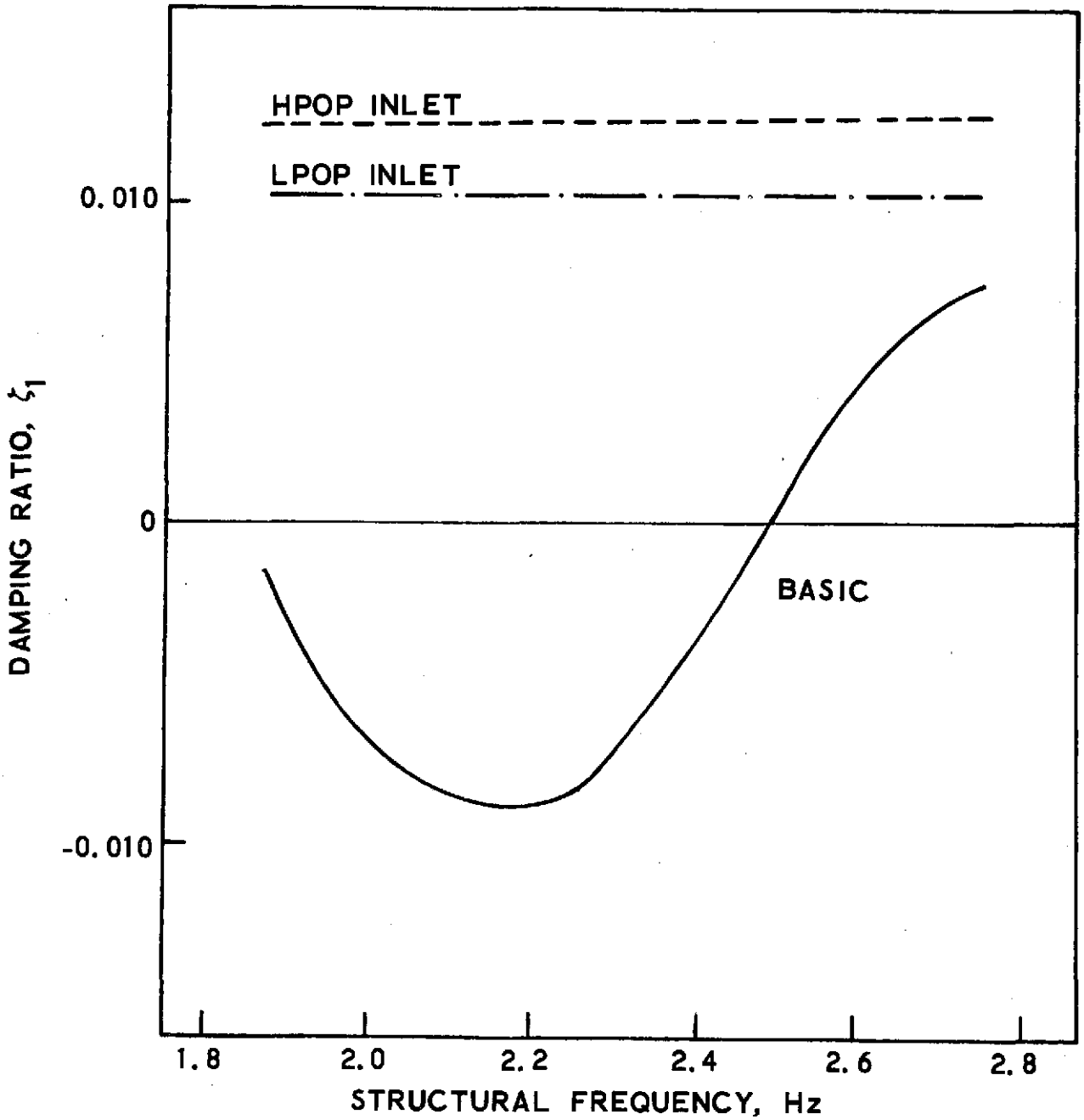

Figure 19. Fundamental mode stability with compliant accumulator: after SRB separation

check was made on the sensitivity of the HPOP-inlet accumulator to reductions in the accumulator volume. The results for a 0.029-m^3 (1 ft^3) accumulator and a 0.014-m^3 (0.5 ft^3) accumulator are shown in figure 20. It is seen that the sensitivity is less than at the liftoff condition. There are reductions in the damping, but the system remains stable with damping ratios in excess of 0.007. With regard to the high-gain forty-sixth mode ($f \sim 27$ Hz), the results (fig. 21) indicated that use of a 0.057-m^3 (2 ft^3) accumulator at the HPOP inlet was beneficial and that use of the LPOP-inlet accumulator produced a decrease in damping with decrease in the structural mode frequency. These trends are similar to those observed in the high-gain structural modes for the other two flight events.

3.3 System With Resistive Accumulator

The design requirements on the 0.057-m^3 (2 ft^3) volume resistive accumulator were Real $Y_a \geq 0.06$ m^5/MN s (1 $in.^2$/sec) for $2 \leq f \leq 30$ Hz. The specific values of the accumulator parameters that were selected to meet this requirement were

$$R_a = 1.7 \text{ MN s/m}^5 \text{ (0.1 sec/in.}^2\text{)}$$

$$L_a = 0.023 \text{ MN s}^2\text{/m}^5 \text{ (0.00133 sec}^2\text{/in.}^2\text{)}$$

As noted previously, the selected values were judged to be practically achievable on the basis of Delta Stage I vehicle experience (ref. 1). In addition to this particular design, three other resistive accumulator designs were briefly examined to determine the sensitivity of the stability results to change in the accumulator parameters.

3.3.1 Propulsion-System Modes

The propulsion-system modes for the various resistive accumulator configurations are quite similar to the modes that were previously calculated for the corresponding compliant accumulator cases, the main differences in the results being an increase in the damping of the feedline-type modes for the case of the LPOP-inlet location.

3.3.2 Selection of Cases

With the exception of some of the less interesting modal cases at liftoff, the same set of stability cases was employed as was used in the study of the compliant accumulator. The deletion of some of the modes at the liftoff condition (the eighteenth, twenty-sixth, and forty-ninth modes were dropped) was done to reduce the proliferating number of stability cases.

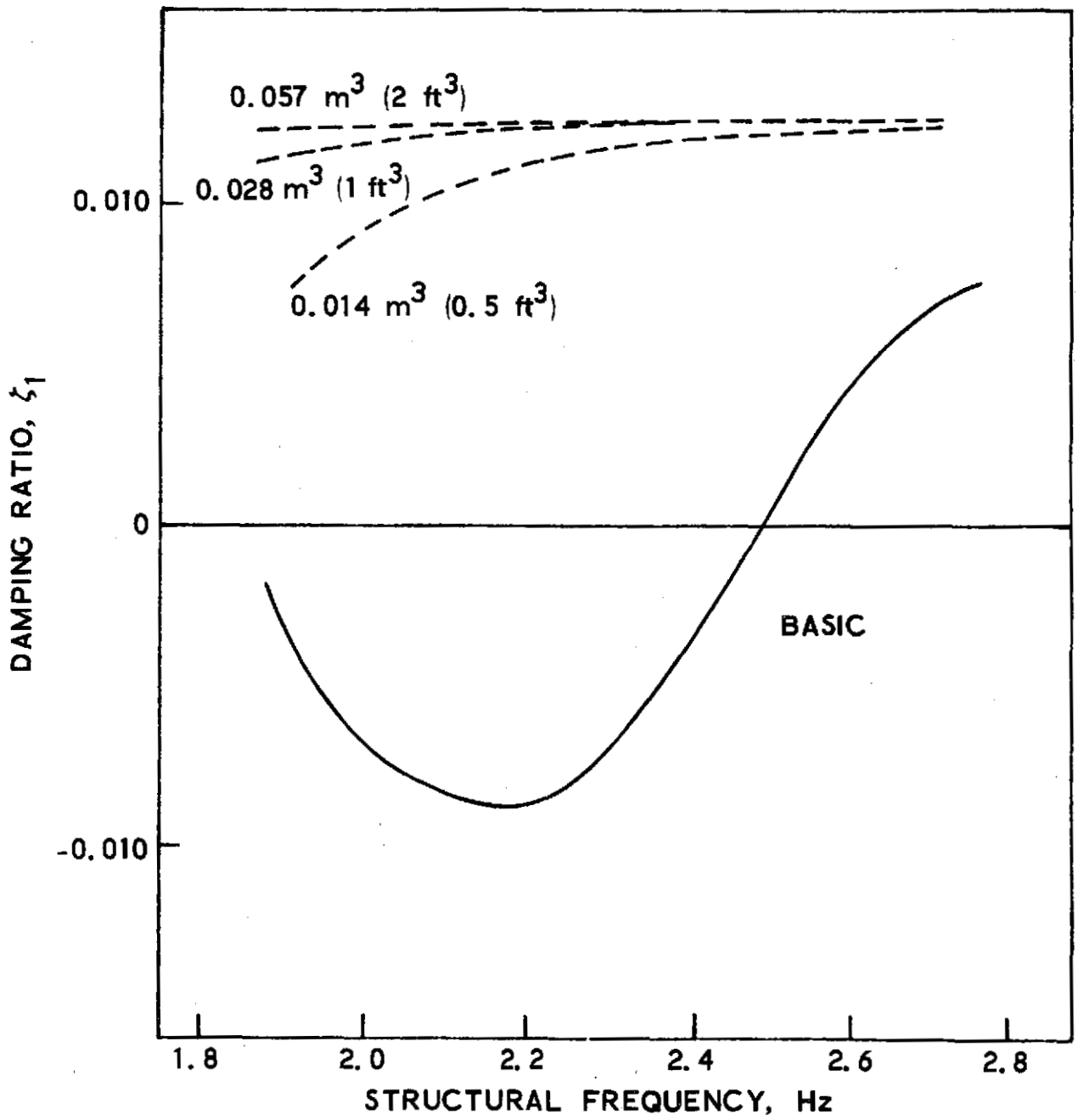

Figure 20. Variation of stability with compliant accumulator volume for HPOP inlet location: after SRB separation

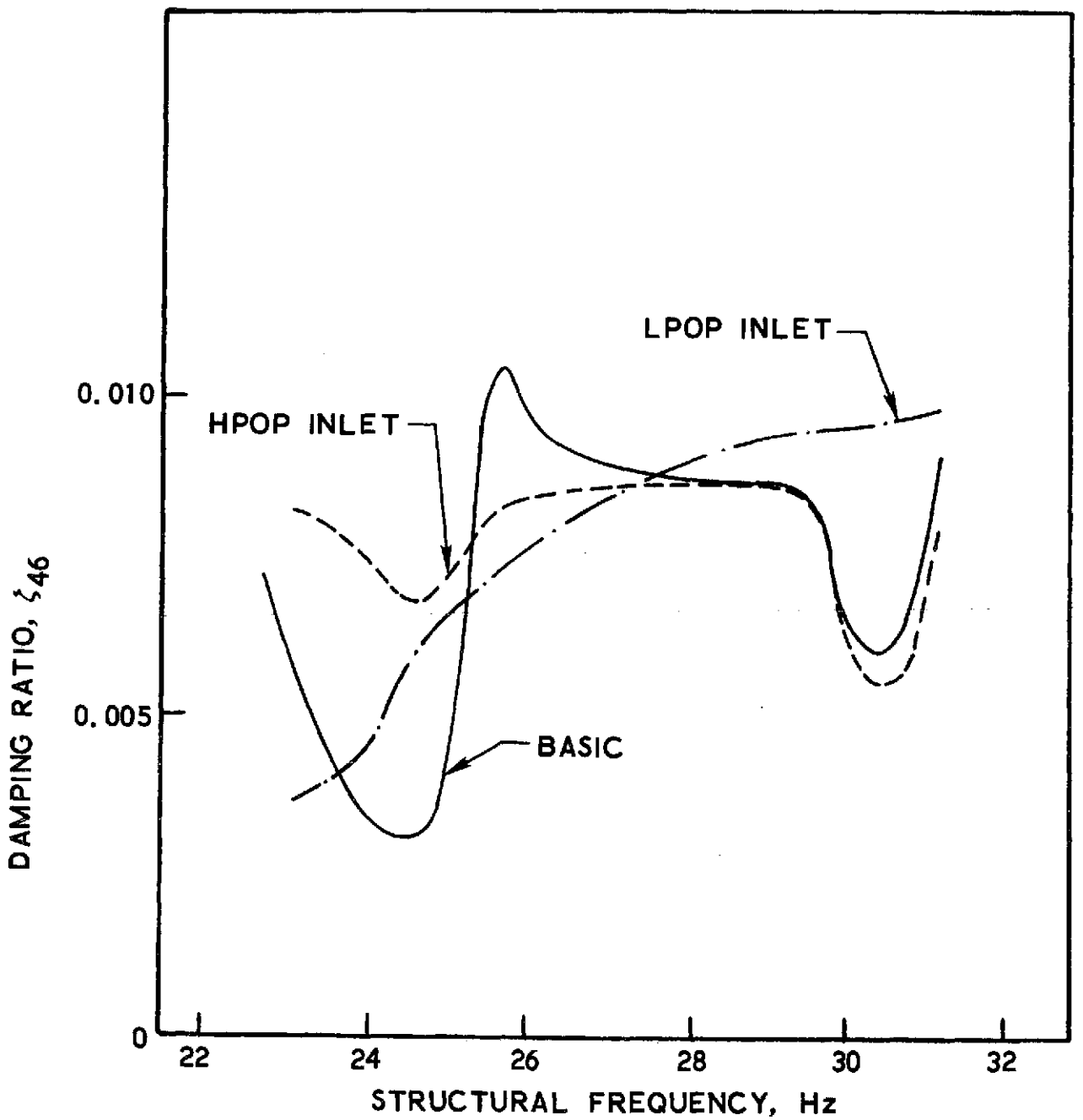

Figure 21. Stability results with compliant accumulator: after SRB separation

3.3.3 Stability Results

3.3.3.1 Orbiter End-Burn

In the case of the first through twenty-first structural modes, the results obtained with the selected resistive accumulator design were found to be essentially identical to the corresponding results obtained with the compliant accumulator. In the case of the thirtieth ($f \sim 22$ Hz) structural mode, there were some slight differences between the resistive and compliant accumulator results, the differences being more pronounced for the LPOP-inlet location.

The results for the thirty-fourth and thirty-fifth modes ($f \sim 27$ Hz) with a resistive accumulator at the LPOP inlet are shown in figures 22a and 22b. Comparison of these results with the corresponding curves for a compliant accumulator at the LPOP inlet (figs. 14a and 14b) show a pronounced difference, in that the variation of damping ratio with structural frequency is no longer monotonic. Since the stability picture in these modes is largely controlled by the interaction between the structural mode and the interpump mode of the propulsion system, it is believed that the differences in the resistive and compliant accumulator results are due to changes on the effective boundary condition on this interpump mode at the LPOP. In contrast to the LPOP-inlet location, the results obtained for a resistive accumulator at the HPOP inlet (figs. 22c and 22d) are very similar to those obtained with the compliant accumulator (figs. 14a and 14b).

The net result of these resistive accumulator analyses was to indicate that the stability picture was essentially unchanged from that predicted for the compliant case. The lower structural modes remained stable; the instability in the thirty-fifth mode was eliminated by use of the accumulator at the HPOP inlet but was not eliminated by use of a resistive accumulator at the LPOP inlet.

In this latter case, the suggestion could be raised that the ineffectiveness of the resistive accumulator at the LPOP inlet was peculiar to the particular design used in the analysis. To investigate this possibility, stability analyses were undertaken with the following additional resistive accumulator designs.

$$\text{Real } Y_a \geq 0.06 \text{ m}^5/\text{MN s} \qquad L_a = 0.023 \text{ MN s}^2/\text{m}^5, \quad R_a = 15 \text{ MN s/m}^5 \tag{a}$$

$$L_a = 0.034 \text{ MN s}^2/\text{m}^5, \quad R_a = 8.5 \text{ MN s/m}^5 \tag{b}$$

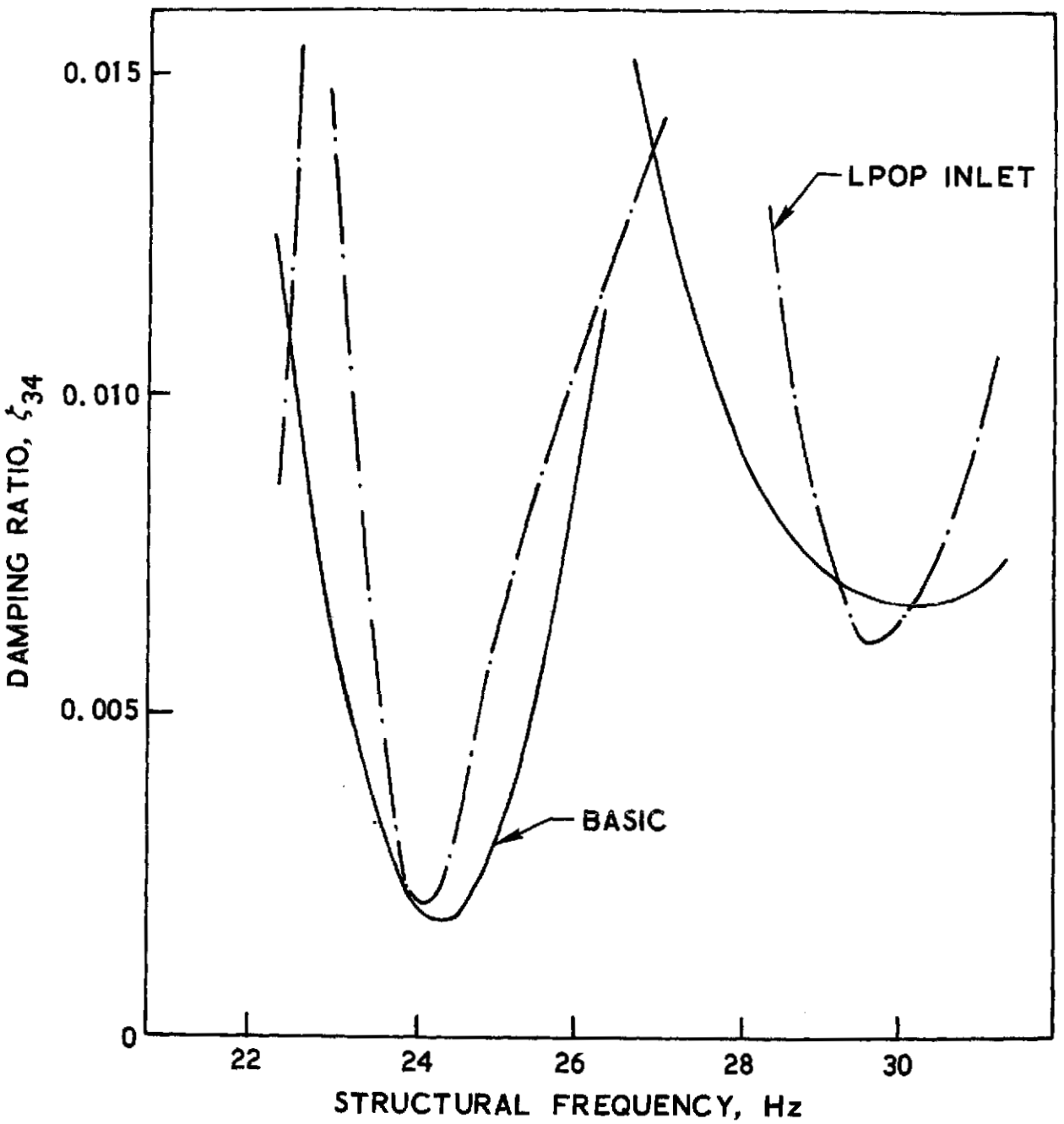

Figure 22a. Stability results with resistive accumulator: orbiter end-burn

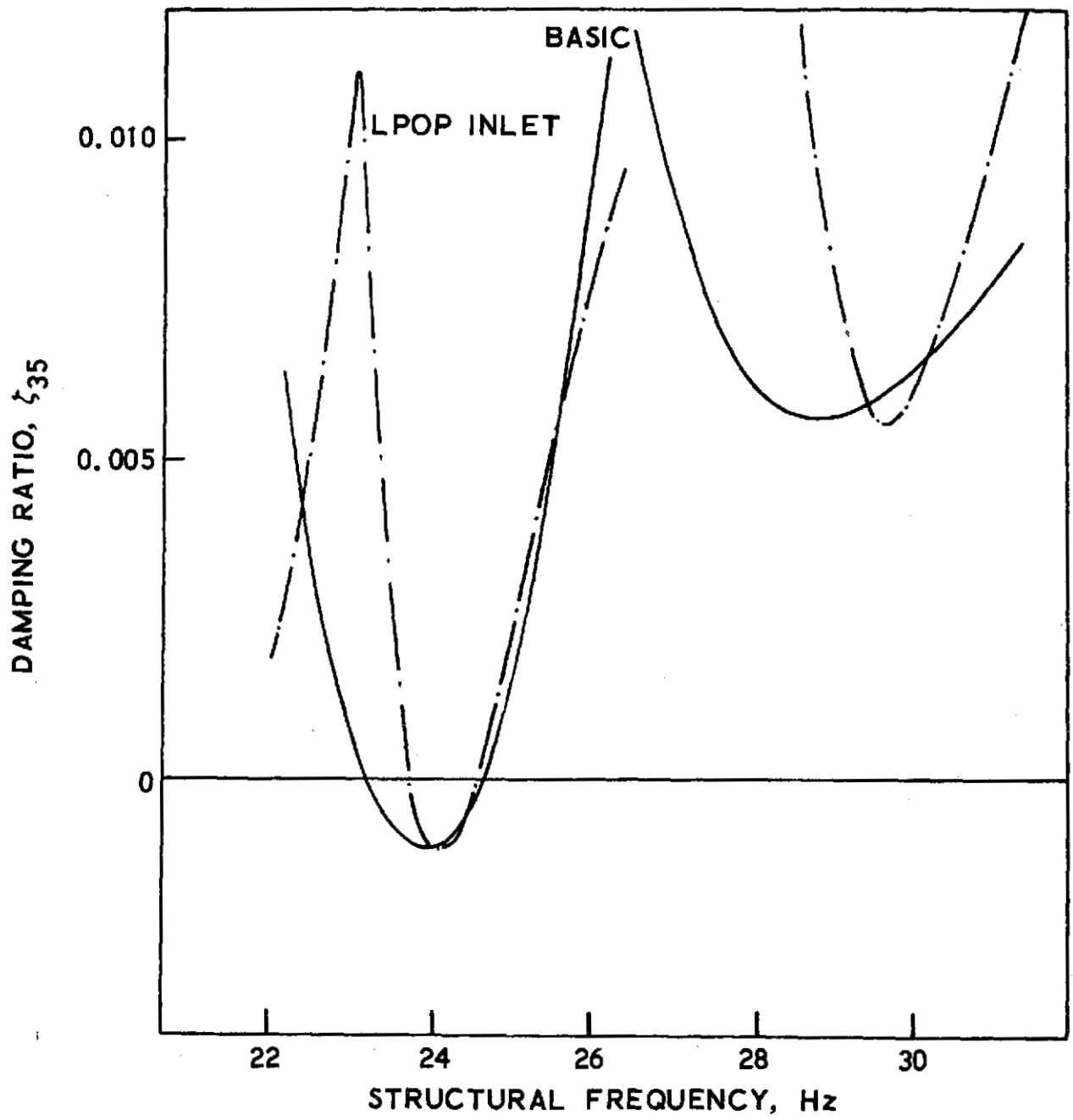

Figure 22b. Stability results with resistive accumulator: orbiter end-burn

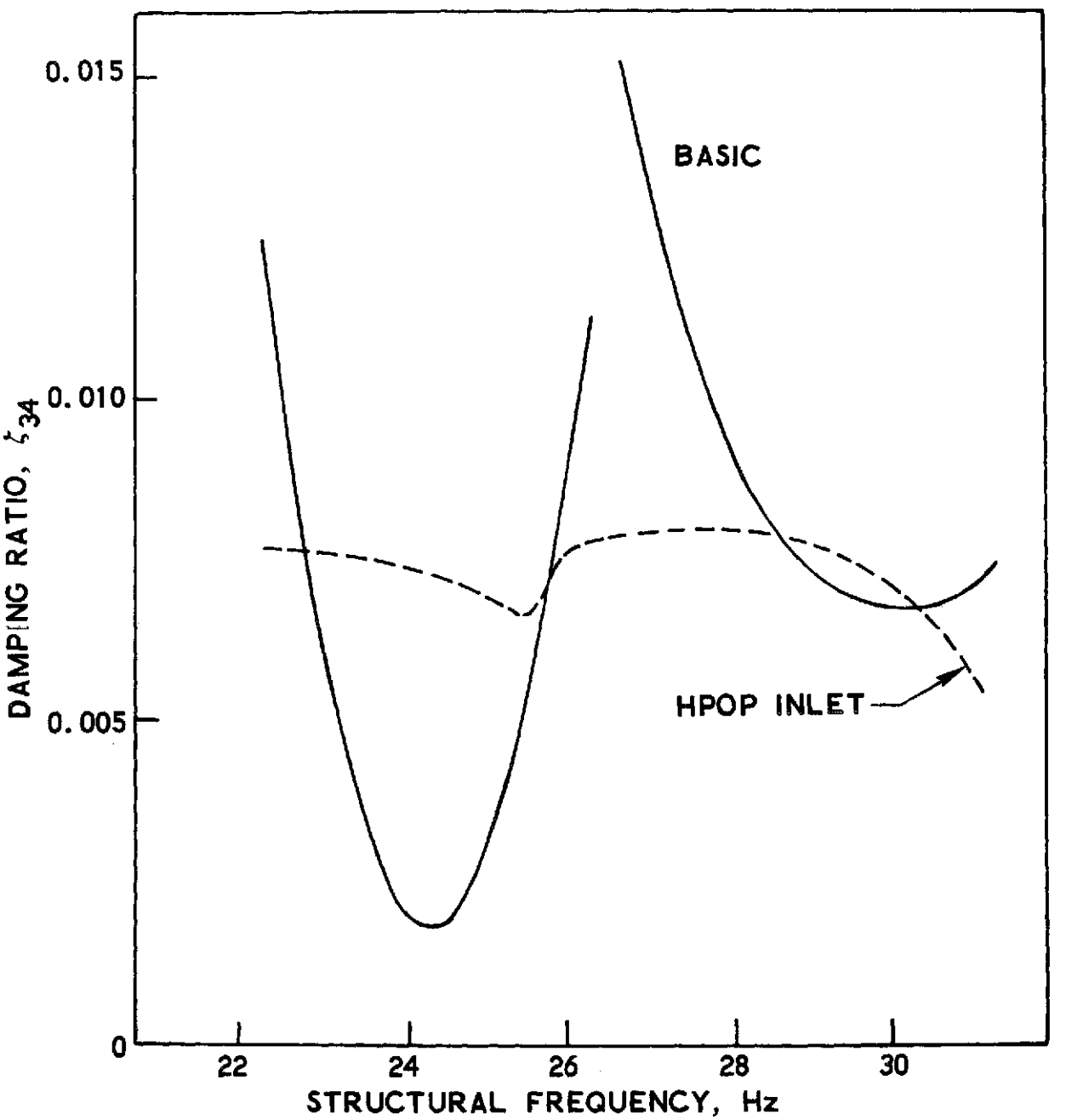

Figure 22c. Stability results with resistive accumulator: orbiter end-burn

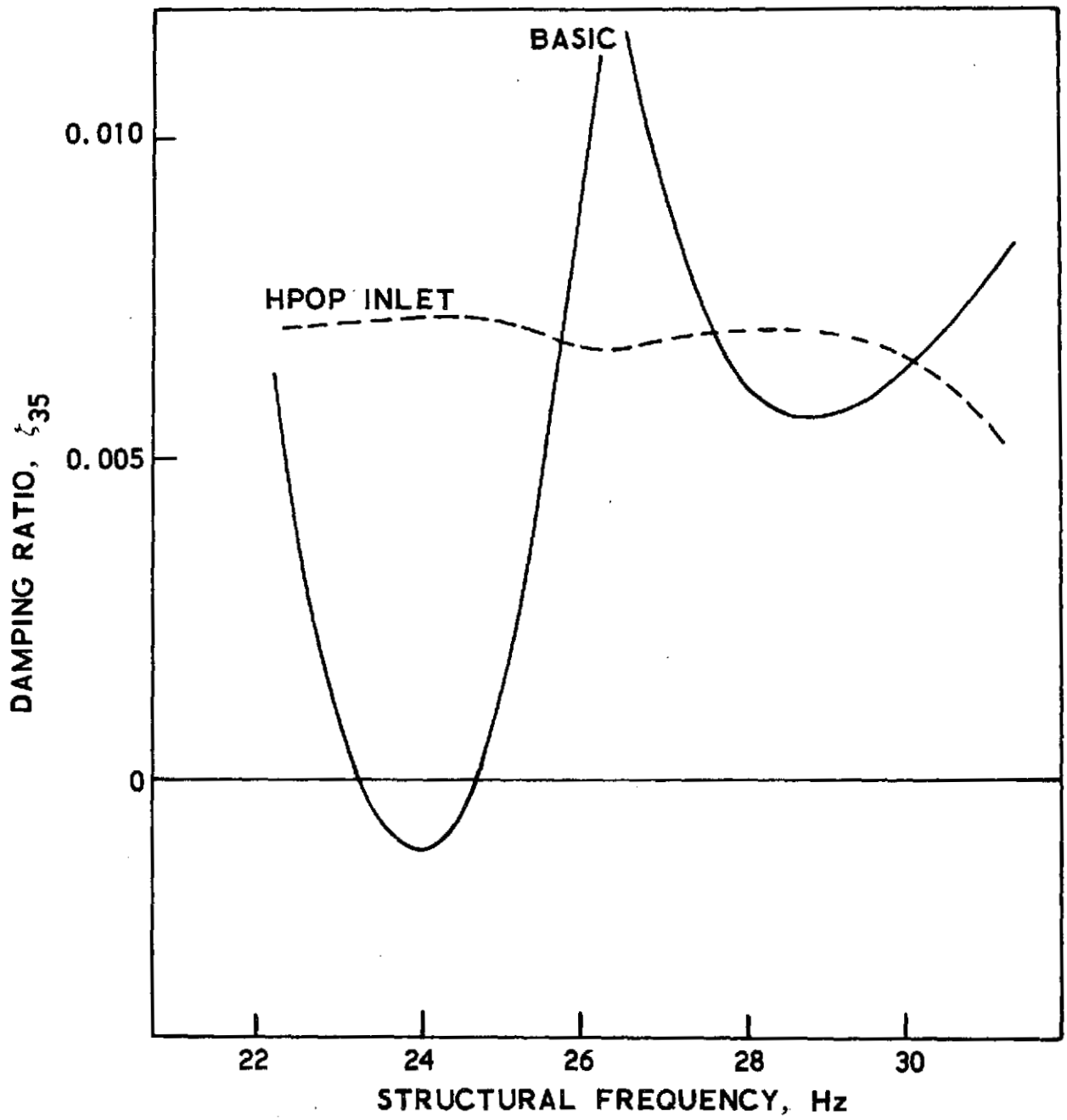

Figure 22d. Stability results with resistive accumulator: orbiter end-burn

$$\text{Real } Y_a \geq 0.3 \text{ m}^5/\text{MN s} \qquad L_a = 0.007 \text{ MN s}^2/\text{m}^5$$
$$R_a = 1.7 \text{ MN s}/\text{m}^5 \qquad \text{(c)}$$

The results obtained with these accumulators at the LPOP inlet were similar to the previous results for the thirty-fifth mode and the instability was not eliminated. Thus, the results indicated that the ineffectiveness of the accumulator at the LPOP inlet was due to the location rather than to the particular accumulator design.

Finally, a limited study was made to see if reduction in the volume of the resistive accumulator, located at the HPOP inlet, would reduce its effectiveness in eliminating the thirty-fifth mode instability. Calculations were made for a 0.028-m^3 (1 ft^3) volume accumulator and a 0.014-m^3 (0.5 ft^3) accumulator. The resulting damping ratios were very close to the results for the 0.057-m^3 (2 ft^3) volume accumulator thereby indicating that these volume reductions did not degrade the effectiveness of the accumulator insofar as elimination of the interpump mode instability was concerned.

3.3.3.2 Liftoff

The results for the liftoff condition showed the same general trends as at the orbiter end-burn condition. The calculated damping ratios for the fundamental modes were close to the corresponding compliant accumulator results. In the higher modes, the fifty-first ($f \sim 22$ Hz) and sixty-second ($f \sim 27$ Hz), pronounced differences were found between the resistive and compliant cases for an accumulator at the LPOP inlet. The results in the higher modes for the HPOP inlet location were similar to the corresponding compliant accumulator results. For this location, the effect of reducing the accumulator volume to 0.028 m^3 (1 ft^3) and 0.014 m^3 (0.5 ft^3) was also checked. The results were almost the same as the corresponding curves obtained for the compliant accumulator at the HPOP inlet (fig. 17) indicating that the effectiveness of this device in eliminating the feedline-type instability in the fundamental mode was significantly degraded by a volume reduction to 0.014 m^3 (0.5 ft^3). Again, this degradation in effectiveness is attributed to an insufficient lowering of the frequency of the first propulsion system mode.

3.3.3.3 After SRB Separation

The same general trends were exhibited for this case. The results for the fundamental mode were very close to the compliant accumulator curves (fig. 19) while differences were found in the forty-sixth ($f \sim 27$ Hz) results for an accumulator at the LPOP inlet.

4. SUMMARY AND CONCLUSIONS

This report provides a qualitative assessment of (1) the tendency for pogo instability of the Shuttle vehicle in the absence of suppression devices and (2) the effectiveness of accumulators in counteracting any tendency toward instability. Compliant and resistive accumulators are considered at three positions in the oxidizer system: LPOP inlet and discharge, and HPOP inlet. Stability analysis is performed by means of digitally computing eigensolutions of the equations describing the coupled structure/propulsion system.

Engineering judgment was applied to construct a mathematical model for the study, with due consideration of the preliminary nature of the available data and the level of complexity necessary to deal with the primary aspects required for a stability assessment. Structural modes of vibration for coupled motion in the vehicle pitch plane were obtained from the Rockwell International Space Division. The propulsion system was simplified to the model shown in figure 3. The numerical values of the propulsion system parameters were based upon the primary geometric and dynamic performance features of the actual system as given by drawings and Rocketdyne's dynamic model of the main engine. The best available basis was employed to predict the cavitation compliances of the pumps, which is a method derived from empirical studies of measured compliances of the family of pumps used on Saturn vehicles. The analytical model is especially rigorous with regard to feedline hydraulics in that a continuous representation, including resistance effects, is employed to represent the multiplicity of damped organ-pipe modes. Contributions to the generalized force for a structural mode included frictional forces due to fluid resistance, fluid momentum-type forces, forces at turns in the fluid flow and at area changes, tank outflow effects, as well as engine thrust.

In the course of the study some sixty-six basic combinations of flight condition/structural mode/accumulator were treated in order to develop comparative data. For the purpose of easy reference, the totality of these basic cases is presented in the following table together with an indication of whether the system was stable or unstable. In addition to these basic cases, the effects of particular variations in the compliant and resistive accumulator designs were also examined.

The major findings from this study are as follows:

1. The basic system can undergo instabilities involving a mode of the propulsion system which can basically involve either the interpump mode or a feedline mode.

2. An instability involving the interpump mode is suppressed effectively only by an accumulator located at the HPOP inlet. Such instability can be intensified by an accumulator at the LPOP inlet or discharge.

3. An instability involving a feedline mode can be counteracted effectively by accumulators at either the LPOP inlet or the HPOP inlet.

4. There is no significant difference in the effectiveness of the compliant and resistive accumulators at the HPOP-inlet location. Reduction of the volume of either type of accumulator at the HPOP inlet to below 0.03 m^3 (1 ft^3) significantly degraded its effectiveness in suppressing feedline-mode instabilities. This same reduction of volume did not significantly degrade the effectiveness of either type of accumulator in suppressing the interpump mode of instability.

Event	Mode	Basic	Compliant			Resistive	
			1	2	3	1	3
Orbiter End-Burn	E1						
	E2						
	E7						
	E21	NA	NA	NA		NA	
	E30						
	E34			X			
	E35	X	X	X		X	
Liftoff	L1	X					
	L18					NA	NA
	L26					NA	NA
	L49					NA	NA
	L51						
	L62						
After SRB SEP	A1	X					
	A46						

Suppressor Location 1 LPOP Inlet

2 LPOP Discharge

3 HPOP Inlet

X - calculated instability

NA - no analysis

With due recognition of the preliminary nature of the analysis, the primary conclusion of this study is believed to be valid: effective pogo suppression can be accomplished using an accumulator at the HPOP-inlet location, but not at the LPOP locations. The determination of which of the two basic types of accumulators, compliant or resistive, is best must await more detailed studies. It is particularly significant that future studies deal with the physical separation of the accumulator from the HPOP inlet, as dictated by engine functional and geometric considerations.

With respect to tentative design requirements, it appears that an accumulator volume of between 0.03 m^3 (1 ft^3) to 0.06 m^3 (2 ft^3) would be appropriate for the compliant device. The same volume range together with the condition Real $Y_a \geq 0.06$ m^5/MN (1 $in.^2/sec$) appears to be adequate for the resistive accumulator.

5. FUTURE STUDIES

It is recommended that the study of passive suppression devices within the engine be continued and that both compliant and resistive accumulators be treated. It is recommended that the analytical model be upgraded by

1. Use of a three-engine representation of the propulsion system that incorporates the ducting between the engines
2. Use of updated structural-mode data and representation of the gimballing degree of freedom of the engines
3. Consideration of the physical separation between the accumulator and the pump inlet

Two additional factors that will require consideration at a later stage of the pogo stability analysis are the three-dimensional character of the interpump ducting and the effect of mechanical resonances of this ducting on the stability picture. Recently, it has been tentatively concluded that mechanical resonances on similar pump discharge ducting of the Delta Stage I vehicle are contributing significantly to observed instabilities.

In the event that a physical design of a resistive accumulator is undertaken, analytical and experimental studies will be required to ensure linear resistive behavior; nonlinear resistive behavior was encountered with the orificed liquid flow in the accumulator employed on the Delta Stage I vehicle. An alternative is the nonlinear resistive device which would entail accumulator testing within the operating engine environment to measure the random flow fluctuations into the accumulator and their effect on the accumulator resistance. This random flow has a considerable bearing on orifice resistance for small superimposed sinusoidal flow fluctuations.

APPENDIX A

SYSTEM EQUATIONS

A. 1 Fluid Dynamic Equations for Propulsion System

The fluid dynamic equations for the individual elements of the propulsion system model are given below.

First Feedline Segment

$$P_1 = \alpha_{11} P_t + \alpha_{12} Q_t + \alpha_{13} \dot{x}_{\ell 1}$$

$$Q_1 = \alpha_{21} P_t + \alpha_{22} Q_t + \alpha_{23} \dot{x}_{\ell 1}$$

First Feedline Corner

$$P_1 = P_2$$

$$Q_2 - A_2 \dot{z}_1 = Q_1 + A_1 \dot{x}_1$$

Second Feedline Segment

$$P_3 = \tilde{\alpha}_{11} P_2 + \tilde{\alpha}_{12} Q_2 - \tilde{\alpha}_{13} \dot{z}_{\ell 2}$$

$$Q_3 = \tilde{\alpha}_{21} P_2 + \tilde{\alpha}_{22} Q_2 - \tilde{\alpha}_{23} \dot{z}_{\ell 2}$$

Second Feedline Corner

$$P_3 = P_4$$

$$Q_4 + A_2 \dot{x}_3 = Q_3 - A_2 \dot{z}_3$$

Low-Pressure Pump

$$Q_5 - A_3 \dot{z}_4 = (Q_4 + A_2 \dot{x}_4) + Q_{A1} - sC_{b1} P_4$$

$$P_5 = (m_1 + 1) P_4 - Z_{p1} Q_5 + R_{p1} A_3 \dot{z}_4$$

LPOP Discharge Suppressor

$$Q_6 - A_3\dot{z}_4 = Q_5 - A_3\dot{z}_4 + Q_{A2}$$

$$P_5 = P_6$$

Interpump Line

$$P_6 - P_7 = Z_i Q_6 - A_3 R_i \dot{z}_7$$

$$Q_6 = Q_7$$

High-Pressure Pump

$$Q_8 - A_4\dot{z}_7 = Q_7 - A_3\dot{z}_7 + Q_{A3} - sC_{b2}P_7$$

$$P_8 = (m_2+1)\,P_7 - Z_{p2}Q_8 + R_{p2}A_4\dot{z}_7$$

Discharge Line

$$P_8 - P_9 = Z_d Q_8 - R_d A_4 \dot{z}_7$$

$$Q_9 = Q_8$$

Injector and Chamber

$$P_9 - P_c = Z_j Q_9 - R_j A_4 \dot{z}_7$$

$$P_c = R_c(Q_9 - A_4\dot{z}_7)$$

In the above equations, A_i, Q_i and P_i denote the flow areas, absolute volume flows, and pressure perturbations at various locations within the system. The Q_{Ai} denote the volume flows from the pogo suppression devices: (m_1+1) and (m_2+1) are the LPOP and HPOP gains; C_{b1} and C_{b2} denote the cavitation compliance at the inlets to the LPOP and HPOP, respectively, while s is the Laplace variable; the $\dot{x}_i, \dot{z}_i$ are the longitudinal and lateral velocities of the structure at various points of the system while $\dot{x}_{\ell 1}$ and $\dot{z}_{\ell 2}$ denote the average translational velocities of the two feedline segments. It will be noted that the lateral velocity of the HPOP, thrust and injection chambers are taken to be the same. The individual impedances Z_i that appear in the above

equations are as follows:

First Feedline Segment

$$Z_1 = L_1 s + R_1$$

Second Feedline Segment

$$Z_2 = L_2 s + R_2$$

Low Pressure Pump

$$Z_{p1} = L_{p1} s + R_{p1}$$

High Pressure Pump

$$Z_{p2} = L_{p2} s + R_{p2}$$

Interpump Line

$$Z_i = L_i s + R_i$$

Discharge Line

$$Z_d = L_d s + R_d$$

Injector

$$Z_j = L_j s + R_j$$

The engine impedance that appears in the equations of motion for the combined structural/propulsion system is defined as

$$Z_e = L_e s + R_e$$

where

$$L_e = L_j + L_d + L_{p2}$$

$$R_e = R_j + R_c + R_d + R_{p2}$$

The transmission coefficients for the first feedline segment are defined as follows:

$$\alpha_{11} = \alpha_{22} = \cosh \theta_1$$

$$\alpha_{12} = - Z_1 \frac{\sinh \theta_1}{\theta_1} \qquad \alpha_{13} = - A_1 R_1 \frac{\sinh \theta_1}{\theta_1}$$

$$\alpha_{21} = - \frac{1}{Z_1} \theta_1 \sinh \theta_1 \qquad \alpha_{23} = - \frac{A_1 R_1}{Z_1} (1 - \cosh \theta_1)$$

where θ_1 is defined by

$$\theta_1^2 = s^2 \tau_1^2 \left(1 + \frac{R_1}{s L_1}\right)$$

with $\tau_1 = \ell_1 / a$ where ℓ_1 is the length of the feedline segment and a is the speed of sound in the liquid oxygen. The coefficients, $\tilde{\alpha}_{ij}$, for the second feedline segment are similar with A_1, R_1, Z_1, θ_1 being replaced by A_2, R_2, Z_2, θ_2, respectively.

The volume flow, Q_{Ai}, from the pogo suppression devices are related to the propulsion system and specific suppressor parameters. The precise form of these relationships is given in Section A. 3.

A. 2 Equation of Motion for Structural Mode

The response of the vehicle structure is taken to be in the n^{th} normal mode. The structural motion $\vec{x}$ at some point $\vec{r}$ is written

$$\vec{x} = q_n e^{st} \phi_n(\vec{r})$$

where q_n is the generalized coordinate and $\phi_n(\vec{r})$ is the associated mode shape. For the case that the structural system is defined with closed-bottom tanks, the equation of motion governing q_n is

$$M_n \left| \ddot{q}_n + 2\zeta_n \omega_n \dot{q}_n + \omega_n^2 q_n \right| = \mathscr{P}_n(tb)\dot{Q}_R + P_t A_1 \phi_n^{(x)}(tb) + \sum_i \vec{F}_i \cdot \vec{\phi}_{ni}$$

where $\mathscr{P}_n(tb)$ is the modal tank-bottom pressure and Q_R is the relative volume outflow from the propellant tank. The detailed development of the contribution of the outflow contribution is found in reference 3. From the results of reference 3, the tank-bottom pressure, P_t, is related to the vehicle motion by

$$P_t = \mathscr{P}_n s^2 q_n$$

The $\vec{F}_i$ comprises the drag forces on the feedline segments, the interpump line and the discharge line, the forces at the two feedline corners, the forces on the LPOP and HPOP and the forces on the injector and thrust chamber. The precise form of these various forces is as follows:

Drag on Feedline Segments

$$F_1^{(x)} = \frac{-A_1 R_1}{Z_1} (P_t - P_2 + A_1 L_1 s \dot{x}_{\ell 1})$$

$$F_1^{(z)} = \frac{A_2 R_2}{Z_2} (P_2 - P_4 - A_2 L_2 s \dot{z}_{\ell 2})$$

Drag on Interpump Line

$$F_i^{(z)} = A_3 R (Q_7 - A_3 \dot{z}_7)$$

Drag on Discharge Line

$$F_d^{(z)} = A_4 R (Q_8 - A_4 \dot{z}_7)$$

Forces at First Feedline Corner

$$F_{c1}^{(x)} = - P_2 A_1 - \bar{f} \left(2 \frac{Q_1}{A_1} + \dot{x}_1 \right)$$

$$F_{c1}^{(z)} = - P_2 A_2 - \bar{f} \left(2 \frac{Q_2}{A_2} - \dot{z}_1 \right)$$

Forces at Second Feedline Corner

$$F_{c2}^{(x)} = P_4 A_2 + \bar{f} \left(2 \frac{Q_4}{A_2} + \dot{x}_3 \right)$$

$$F_{c2}^{(z)} = P_4 A_2 + \bar{f} \left(2 \frac{Q_3}{A_2} - \dot{z}_3 \right)$$

Forces at LPOP

$$F_{p1}^{(x)} = - P_4 A_2 - \bar{f} \left(2 \frac{Q_4}{A_2} + \dot{x}_4 \right)$$

$$F_{p1}^{(z)} = - P_5 A_3 - \bar{f} \left(2 \frac{Q_5}{A_3} - \dot{z}_4 \right)$$

Forces at HPOP

$$F_{p2}^{(z)} = P_7 A_3 - P_8 A_4 + 2\bar{f} \left(\frac{Q_7}{A_3} - \frac{Q_8}{A_4} \right)$$

Force at Injector

$$F_i^{(z)} = A_4 P_9$$

Force at Thrust Chamber

$$F_t^{(x)} = A_T P_c$$

In the above expressions $\bar{f}$ denotes the mean mass flow of the propellant

$$\bar{f} = \rho \bar{V} A$$

where ρ is the mass density of the propellant and $\bar{V}$ is the steady flow velocity. The items that involve $\bar{f}$ derive from the convective derivative in the fluid momentum equation.

A.3 Description of Accumulator

The volume flow, Q_A, from an accumulator in the system is written as

$$Q_A = - Y_a P$$

where P is the pressure perturbation at the accumulator; Y_a is the admittance of the accumulator. For a resistive device, it is convenient to express the admittance Y_a in the following form

$$Y_a = \frac{s/L_a}{\left|s^2 + 2\zeta_a \omega_a s + \omega_a^2\right|}$$

where L_a, ζ_a and ω_a denote the inertance, damping ratio and natural frequency of the accumulator, respectively. In the special case of a purely compliant device, it is convenient to write

$$Y_a = C_a s$$

where C_a is the compliance of the accumulator.

APPENDIX B

SHUTTLE LOX SYSTEM PARAMETERS

RESISTANCE,[1]	MN s/m^5	(sec/in.^{2})
R_1 =	0.4	(0.0236)
R_2 =	0.11	(0.0064)
R_{p1} =	8.8	(0.52)
R_{p2} =	44.7	(2.64)

[1] Resistance in SI units is based upon pressure divided by volume flow; in English units, weight flow is employed.

R_i = 1.9 (0.11)

R_e = 156 (9.19)

R_c = 42.3 (2.50)

R_d = 8.3 (0.49)

R_j = 60.2 (3.56)

INERTANCE,[2] MN s^2/m^5 ($sec^2/in.^2$)

L_1 = 0.71 (0.0417)

L_2 = 0.19 (0.0113)

L_{p1} = 0.017 (0.001)

L_{p2} = 0.042 (0.0025)

L_i = 0.22 (0.013)

L_e = 0.38 (0.0225)

L_d = 0.25 (0.015)

L_j = 0.085 (0.005)

CAVITATION COMPLIANCE

C_{b1} =
C_{b2} = } See figure 4

PUMP GAIN

See figure 5

TIMES (sec)

τ_1 =
τ_2 = } 0.0656, 0.0178 Feedline Travel Time

[2]The flow difference in (1) also applies to inertance.

AREAS ($in.^2$)

A_1 = 75.7

A_3 = 31.2

A_4 = 12.6

A_T = 158

REFERENCES

1. Payne, J. G. : Pogo Suppression on the Delta Vehicle. Report No. TR-0074(4704)-1, The Aerospace Corporation, El Segundo, California.

2. Rubin, S. : Longitudinal Instability of Liquid Rockets Due to Propulsion Feedback (POGO). J. Spacecraft Rockets, 3(8), August 1966, pp. 1188-1195.

3. Rubin, S. ; Wagner, R. G. ; Payne, J. G. : Pogo Suppression on Space Shuttle-Early Studies. NASA CR-2210, March 1973.

4. Holt, J. F. : ACS Mule, General Root Finding Subroutine. Report No. TOR-0073(9320)-8, The Aerospace Corporation, El Segundo, California, March 1973.

5. SSME Model, Engine Dynamic Characteristics Related to Pogo. Report No. RSS-8549-2, Rocketdyne Division, Rockwell International, Canoga Park, California, September 1973.

6. Ghahremani, F. G. ; Rubin, S. : Empirical Evaluation of Pump Inlet Compliance. Report No. ATR-73(7257)-1, The Aerospace Corporation, El Segundo, California, August 1972.